Supplementary information

Efficient Implementation of MINT-Based Chemiresistor Arrays for Artificial Olfaction.

Michele Galvani[†], Alejandro López-Moreno[‡], Natalia Martín Sabanés[‡], Sylwia Parzyszek[‡], Michele Zanotti[†], Sonia Freddi[†⊥], Emilio M. Pérez*[‡], Luigi Sangaletti*[†]

[†] Surface Science and Spectroscopy Labs @ I-LAMP, Department of Mathematics and Physics, Università Cattolica del Sacro Cuore, via della Garzetta 48, 25113 Brescia (Italy)

[‡] IMDEA Nanociencia, Faraday 9, 28049 Madrid (Spain)

[⊥] Present address: Institute for Photonics and Nanotechnologies (IFN) - Consiglio Nazionale delle Ricerche (CNR) L-NESS laboratory, via Anzani 42, 22100 Como (Italy)

Email: luigi.sangaletti@unicatt.it; Emilio.perez@imdea.org

1. Materials and methods

All general reagents were obtained from commercial sources and used without further purification. Flash chromatography was performed using silica gel (Merck, Kieselgel 60, 230–240 mesh, or Scharlau 60, 230–240 mesh). The SWCNTs used were commercially available Tuball SWCNTs (99 ± 0.5 wt % SWCNT content, 1.6 ± 0.4 nm diameter, >5 μm length) purchased from OCSiAl.

NMR spectra were recorded on a Bruker Advance 400 (1H: 400 MHz, 13C: 101 MHz) at 298 K using the solvent noted in each case. Coupling constants (J) are denoted in Hz and chemical shifts (δ) in ppm. Multiplicities are denoted as follows: s = singlet, d = doublet, t = triplet, m = multiplet, b = broad. These spectra are shown in the S.I. file.

The extinction spectra were measured in a quartz cuvette (path length = 1 cm) with a Cary 5000 UV/Vis/NIR spectrophotometer.

Thermogravimetric analyses (TGA) were performed using a TA Instruments TGAQ500. The TGA method was set to perform a first equilibration at 50 C during 15 min followed by a ramp of 10 °C/min under air or N2 from 100 to 1000 °C.

Raman spectra on powders were recorded with a Bruker Senterra confocal Raman microscope (Bruker Optic, Ettlingen, Germany, resolution 3–5 cm^{-1}).

SEM micrographs of the sensing layers were obtained in a Zeiss EVO HD15 operating at 3 kV. MicroRaman maps of sensing layers have been collected at a 633 nm laser wavelength, with a Renishaw inVia^{TM} confocal Raman microscope, equipped with an 1800 lines/mm grating, a 100x objective, and a laser power of 10 mW on the sample.

Mechanical grinding was performed with an agate mortar and pestle under ambient conditions and a Fritsch Planetary Micro Mill PULVERISETTE 7 in Steel Reactors of 20 mL

2. Synthesis of U-shape molecules

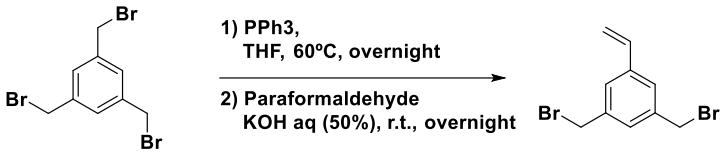

1,3,5-tris(bromomethyl)benzene--1,3-bis(bromomethyl)-5-vinylbenzene. Tri(bromomethyl) benzene (2 g, 5.6 mmol, 1 eq) and triphenylphosphine (1.69 g, 6.45 mmol, 1.15 eq) were dissolved in 28 mL of THF and stirred at 60°C overnight. After this time the reaction was cooled to room temperature and the product was recovered by filtration and washed with THF. The product was dissolved in 20 mL of CH_2Cl_2 and paraformaldehyde (336 mg, 11.2 mmol, 2 eq) and 50% KOH aqueous solution (6 mL) was added and stirred at room temperature overnight. Water was added to the reaction and extracted three times with dichloromethane. Then the solvent was evaporated, and the resulting product was subjected to column chromatography (Hexane: CH_2Cl_2 5:1) to obtain the pure product (980 mg, 60% yield).

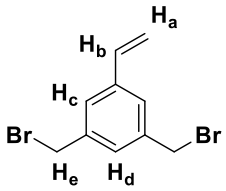

^{1}H NMR (400 MHz, $CDCl_3$) δ 7.35 (d, *J* = 1.8 Hz, 2H, Hc), 7.31 (s, 1H, Hd), 6.68 (dd, *J* = 17.6, 10.9 Hz, 1H, Hb), 5.89 – 5.70 (m, 1H, Ha), 5.32 (d, *J* = 10.9 Hz, 1H, Ha), 4.47 (s, 4H, H_e).

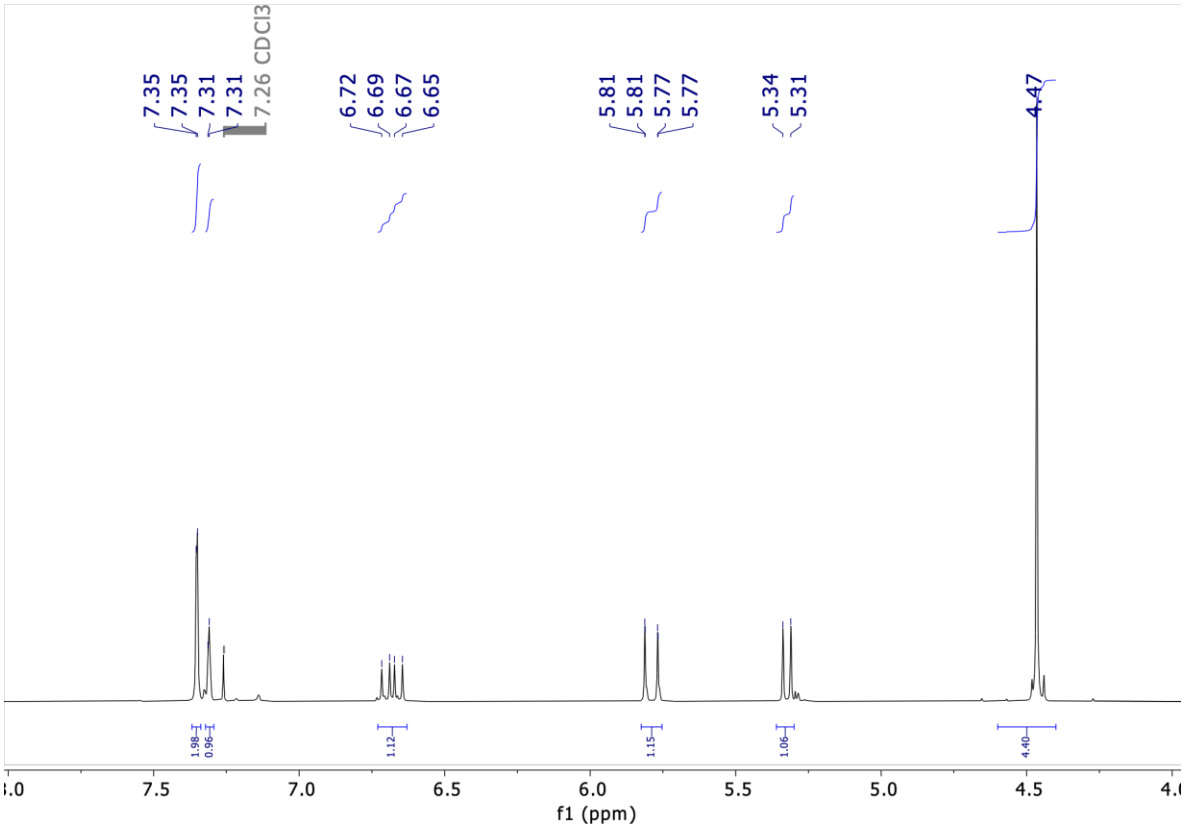

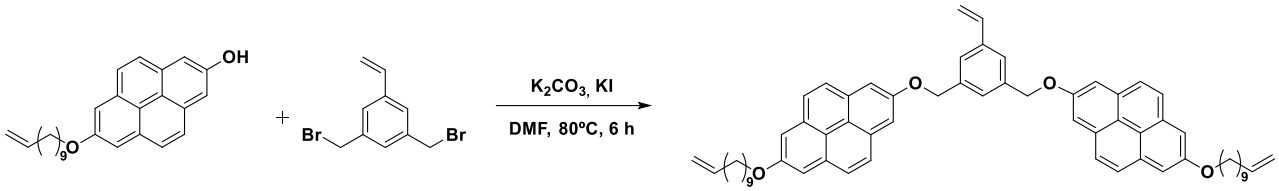

7-(undec-10-en-1-yloxy)pyren-2-ol and 1,4-bis(((7-(undec-10-en-1-yloxy)pyren-2-yl)oxy)methyl)benzene were synthesized as in **[1].**

7,7'-(((5-vinyl-1,3-phenylene)bis(methylene))bis(oxy))bis(2-(undec-10-en-1-yloxy)pyrene). 1.65 g (11.8 mmol, 4.4 eq) of dry K2CO3, 780 mg (2.7 mmol, 1 eq) of 1,3,5-tris(bromomethyl)benzene--1,3-bis(bromomethyl)-5-vinylbenzene, and a catalytic amount of potassium iodide were added to a solution of 2.24 g (5.79 mmol, 2.2 eq) of pyrene derivative in 60 mL of dry N,N-dimethylformamide. The solution was heated to 80 ºC for 6 h. The crude reaction was poured into ice-cold 1 M aqueous HCl, and filtered. The solid was washed with water and methanol, obtaining a pure product (2.3 g, 95% yield).

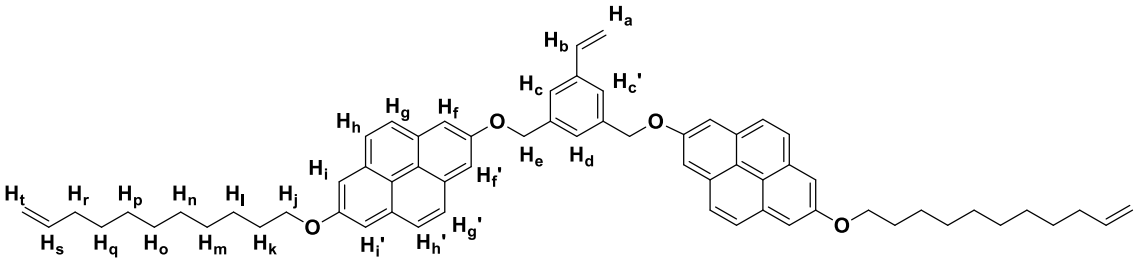

^{1}H NMR (400 MHz, $CDCl_3$) δ 7.91 (s, 8H, Hg+g'+h+h'), 7.75 (s, 4H, Hf+f'), 7.68 (s, 4H, Hi+i'), 7.64 (s, 1H, Hd), 7.59 (d, *J* = 1.7 Hz, 2H, Hc+c'), 6.80 (dd, *J* = 17.6, 10.9 Hz, 1H, Hb), 5.98 – 5.71 (m, 3H, Ha+s), 5.38 (s, 4H, He), 5.36 – 5.25 (m, 1H, Ha), 5.12 – 4.73 (m, 4H, Ht), 4.24 (t, *J* = 6.5 Hz, 4H, Hj), 2.11 – 2.00 (m, 4H, Hr), 1.99 – 1.86 (m, 4H, H_k), 1.56 (q, *J* = 7.5 Hz, 8H, Hl+q), 1.45 – 1.19 (m, 16H, Hm+n+o+p).^{13}C NMR (101 MHz, $CDCl_3$) δ 157.0, 156.4, 139.4, 138.7, 138.2, 137.8, 136.6, 131.8, 131.7, 128.1, 127.7, 127.6, 126.1, 125.1, 120.5, 120.1, 115.0, 114.3, 111.7, 111.5, 70.5, 68.8, 34.0, 29.7, 29.6, 29.6, 29.5, 29.3, 29.1, 26.3. MALDI calcd. for C64H68O4 (M): 900.5; Found: 900.5.

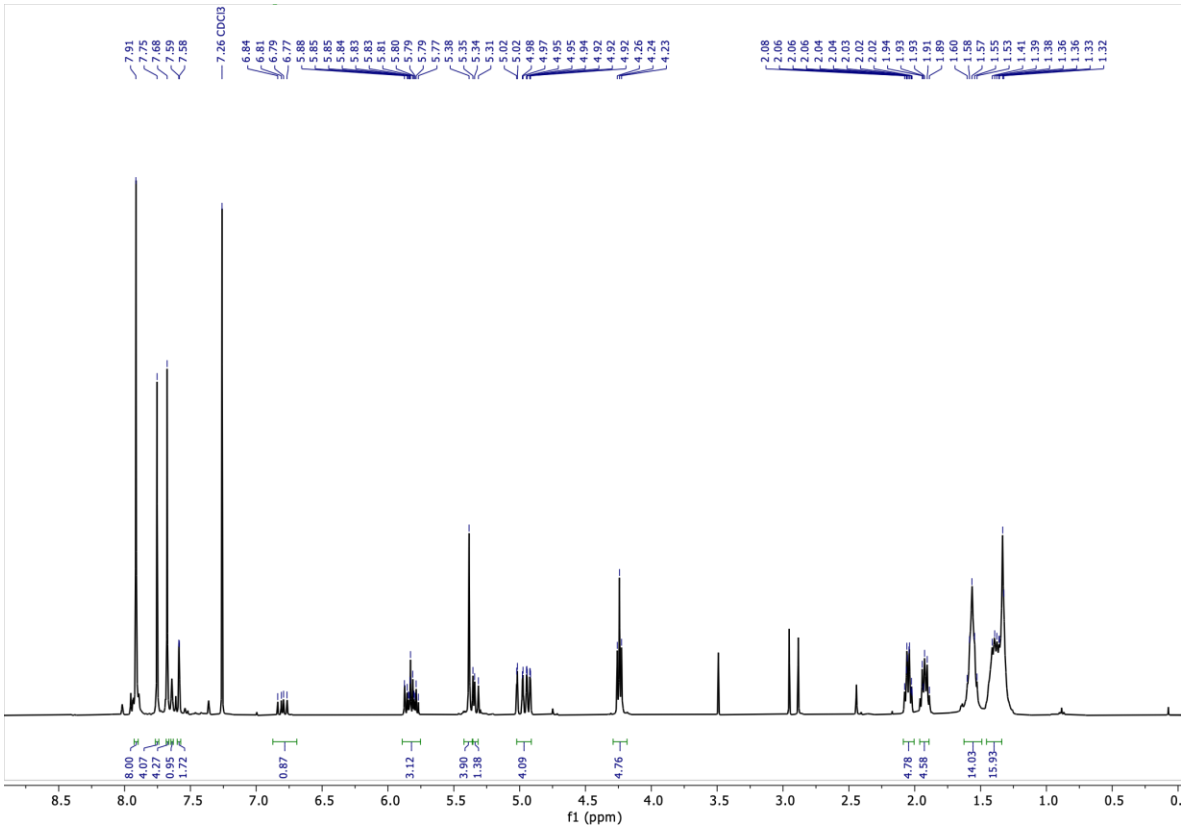

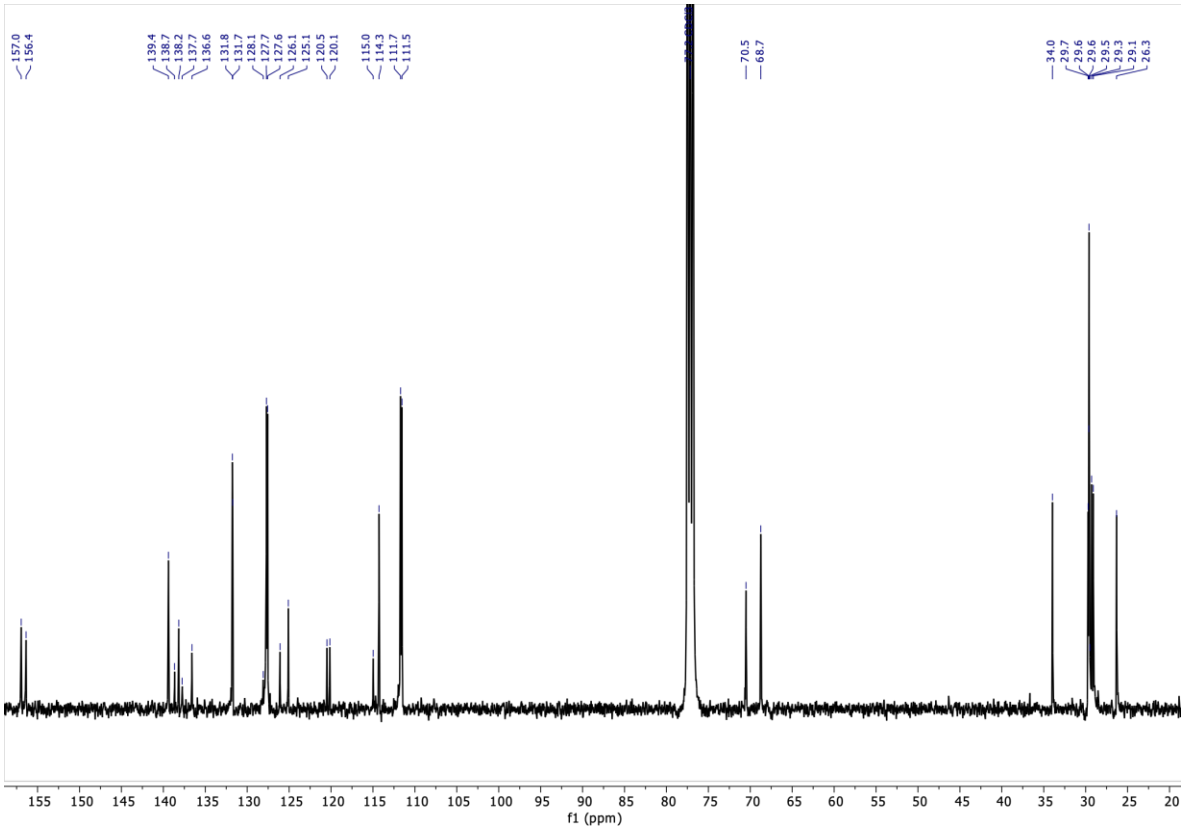
157.0
156.4
139.4
138.7
138.2
137.7
136.6
131.8
131.7
128.1
127.7
127.6
126.1
125.1
120.5
120.1
115.0
114.3
111.7
111.5
70.5
68.7
34.0
29.7
29.6
29.6
29.5
29.3
29.1
26.3
f1 (ppm)

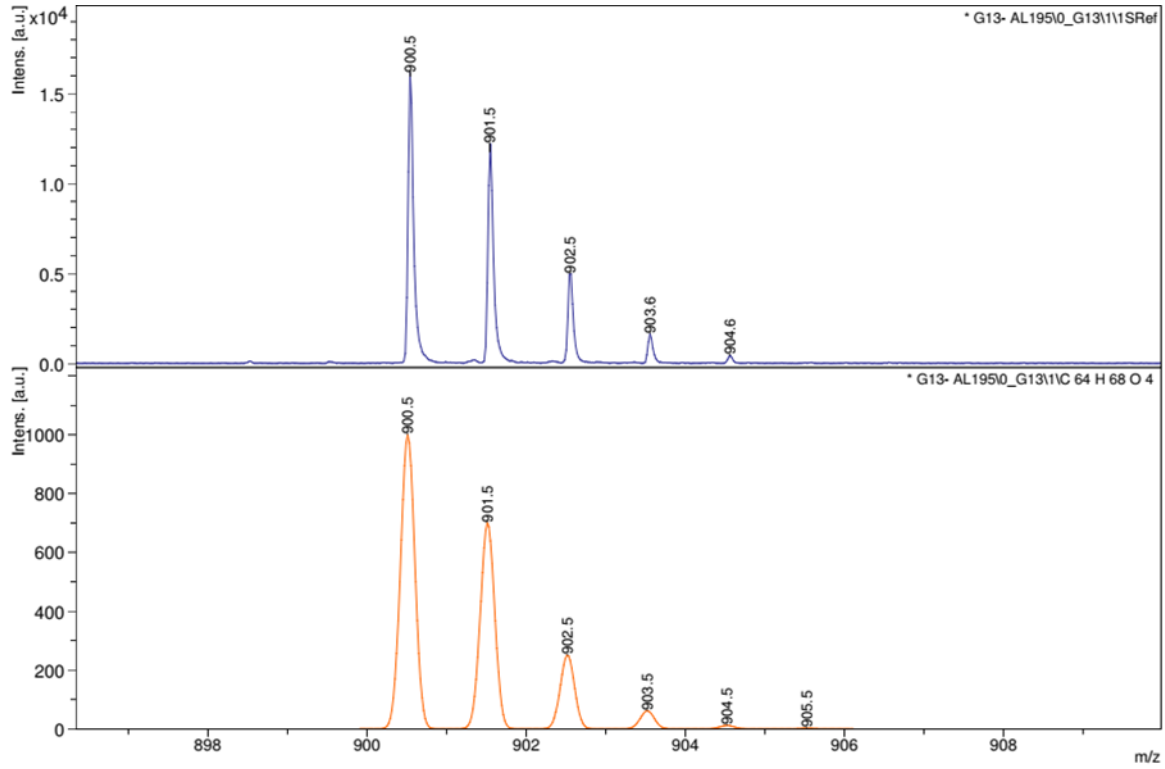
* G13- AL195\0_G13\1\1SRef
Intens. [a.u.]
x10^4
900.5
901.5
902.5
903.6
904.6
* G13- AL195\0_G13\1\C 64 H 68 O 4
Intens. [a.u.]
900.5
901.5
902.5
903.5
904.5
905.5
m/z

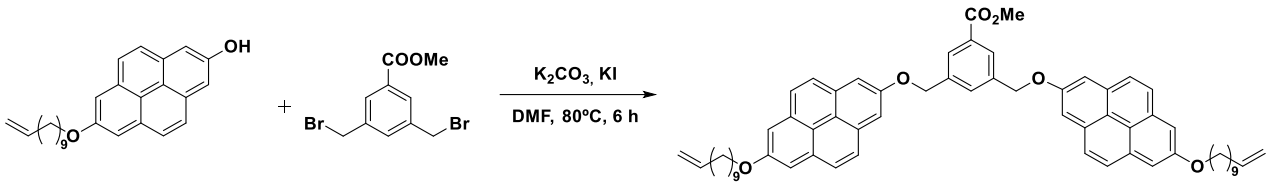

methyl 3,5-bis(((7-(undec-10-en-1-yloxy)pyren-2-yl)oxy)methyl)benzoate. 1.44 g (10.3 mmol, 4.4 eq) of dry K2CO3, 750 mg (2.35 mmol, 1 eq) of methyl 3,5-bis(bromomethyl)benzoate, and a catalytic amount of potassium iodide were added to a solution of 2 g (5.18 mmol, 2.2 eq) of pyrene derivative in 55 mL of dry N,N-dimethylformamide. The solution was heated to 80 ºC for 6 h. The crude reaction was poured into ice-cold 1 M aqueous HCl, and filtered. The solid was washed with water and methanol obtaining pure product (2 g, 92% yield).

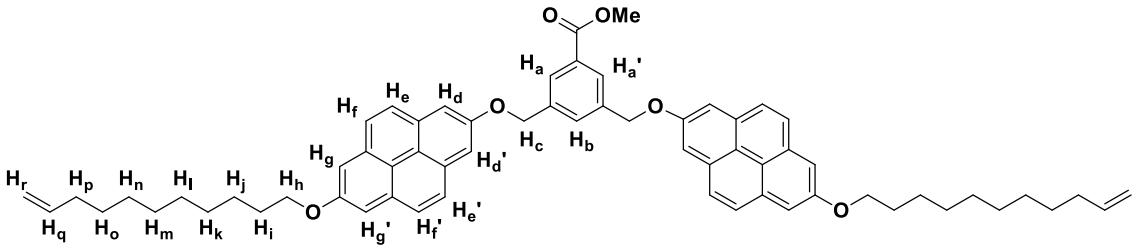

^{1}H NMR (400 MHz, $CDCl_3$) δ 8.22 (d, *J* = 1.8 Hz, 2H, Ha+a'), 7.96 (s, 1H, Hb), 7.94 – 7.87 (m, 8H, He+e'+ f+f' , 7.73 (s, 4H, Hd+d'), 7.67 (s, 4H, Hg+g'), 5.82 (ddt, *J* = 16.9, 10.1, 6.7 Hz, 2H, Hq), 5.42 (s, 4H. Hc), 5.10 – 4.86 (m, 4H, Hr), 4.24 (t, *J* = 6.6 Hz, 4H, Hh), 3.96 (s, 3H, -OMe), 2.05 (tdd, *J* = 6.6, 5.3, 1.5 Hz, 4H, Hp), 1.92 (dt, *J* = 14.7, 6.6 Hz, 4H, Hi), 1.55 (m, 8H, Ho+j), 1.48 – 1.33 (m, 16H, Hk+l+m+n). ^{13}C NMR (101 MHz, CDCl3) δ 166.9, 157.0, 156.1, 139.4, 138.4, 131.8, 131.7, 131.2, 130.9, 128.2, 127.8, 127.5, 120.5, 120.1, 114.3, 112.0, 111.7, 111.6, 70.0, 68.7, 52.5, 34.0, 29.7, 29.6, 29.3, 29.1, 26.3. MALDI calcd. for C64H68O6 (M): 932.5; Found: 932.5.

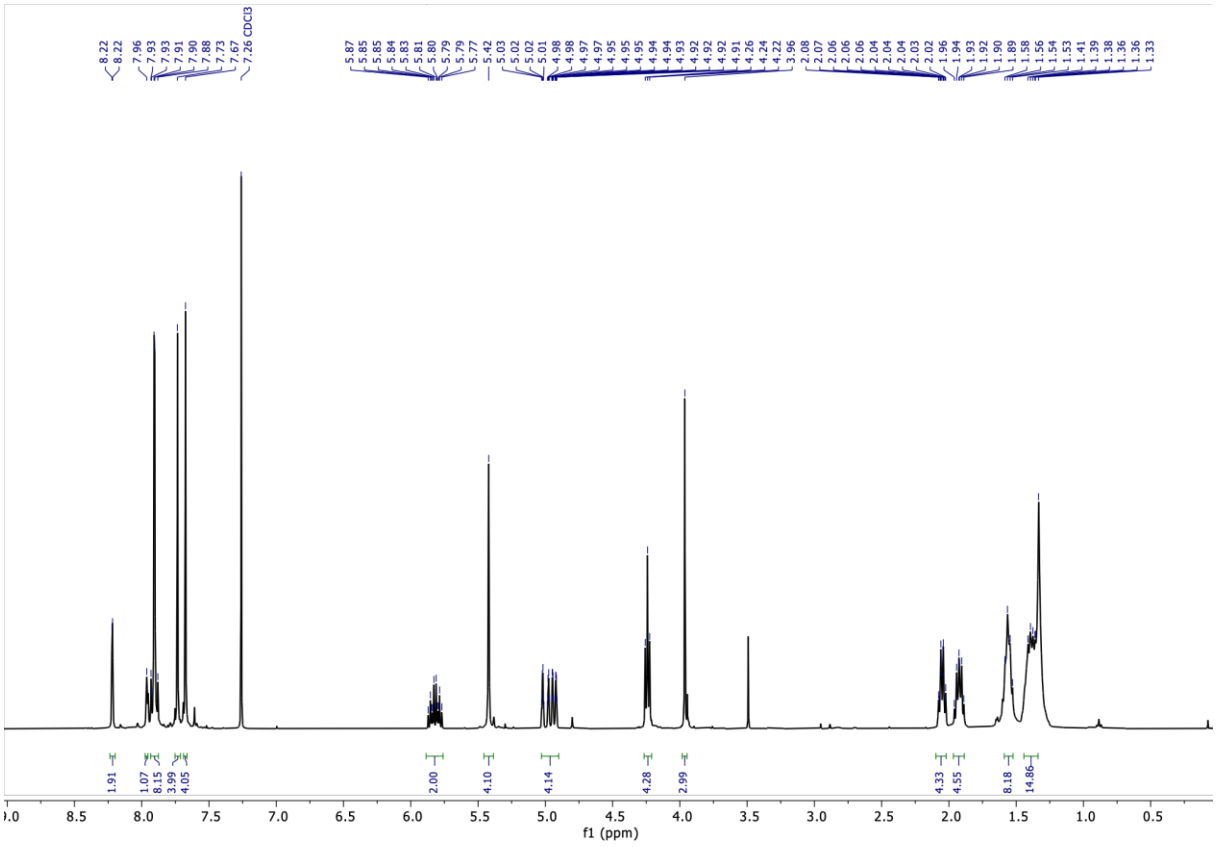

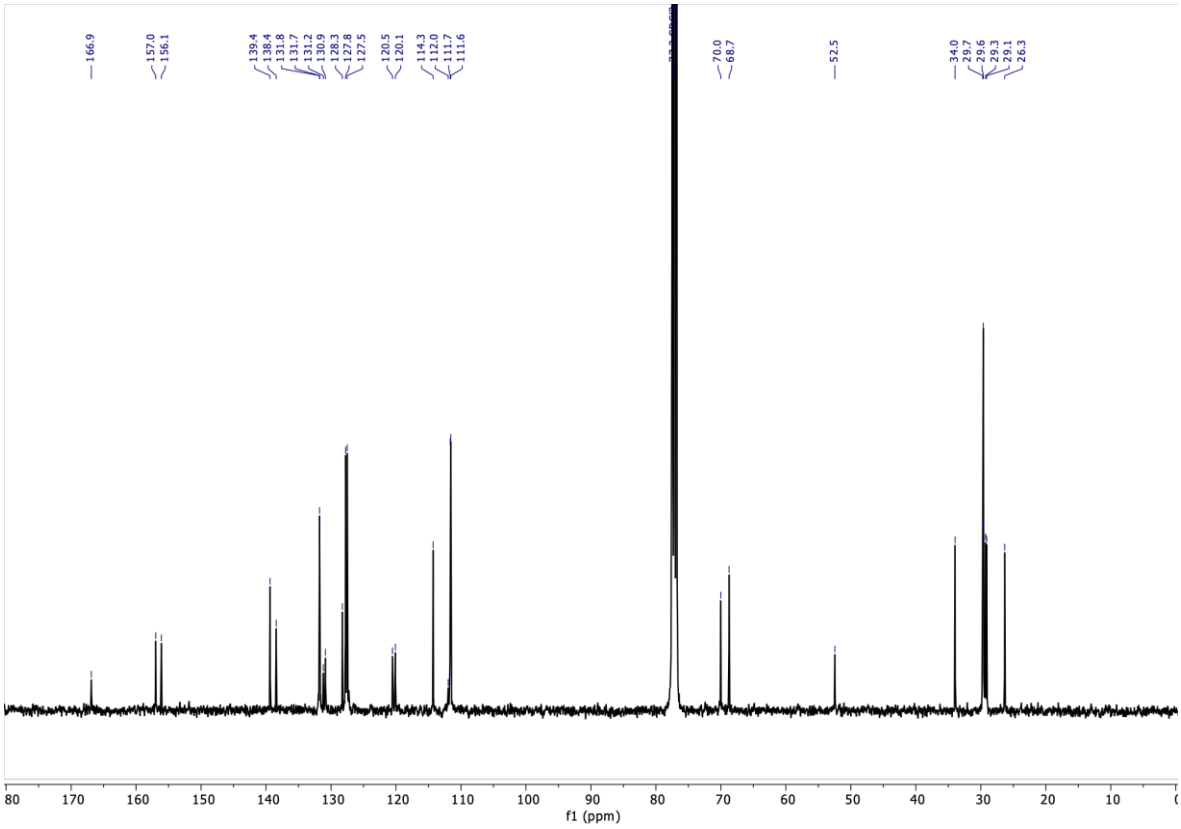
166.9
157.0
156.1
139.4
138.4
131.8
131.7
131.2
130.9
128.3
127.8
127.5
120.5
120.1
114.3
112.0
111.7
111.6
70.0
68.7
52.5
34.0
29.7
29.6
29.3
29.1
26.3
f1 (ppm)

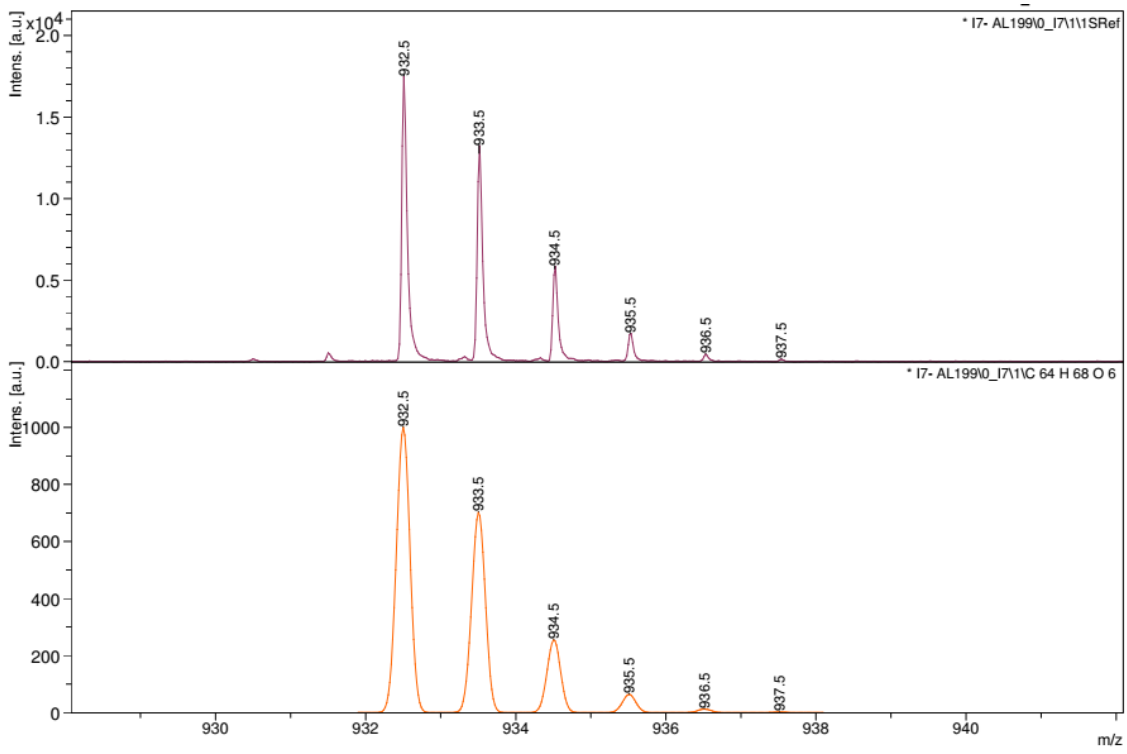
* I7- AL199\0_I7\1\1SRef
Intens. [a.u.]
x10^4
932.5
933.5
934.5
935.5
936.5
937.5
* I7- AL199\0_I7\1\C 64 H 68 O 6
m/z

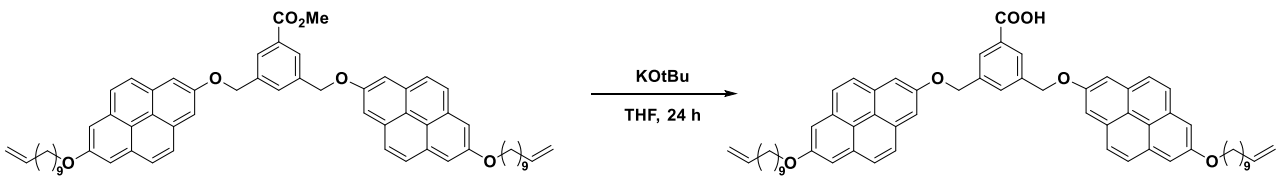
CO2Me
KOtBu
THF, 24 h
COOH

3,5-bis(((7-(undec-10-en-1-yloxy)pyren-2-yl)oxy)methyl)benzoic acid. methyl 3,5-bis(((7-(undec-10-en-1-yloxy)pyren-2-yl)oxy)methyl)benzoate (250 mg, 0.27 mmol, 1 eq) was dissolved in 20 mL of THF. Over this solution 82 mg (0.73 mmol, 2.7 eq) of potassium *tert*butoxide were added and the reaction was stirred for 24 h at room temperature. After this time HCl 1M was added and the product was extracted with chloroform. Solvent was removed under vacuum obtaining 242 mg (97% yield) of pure product.

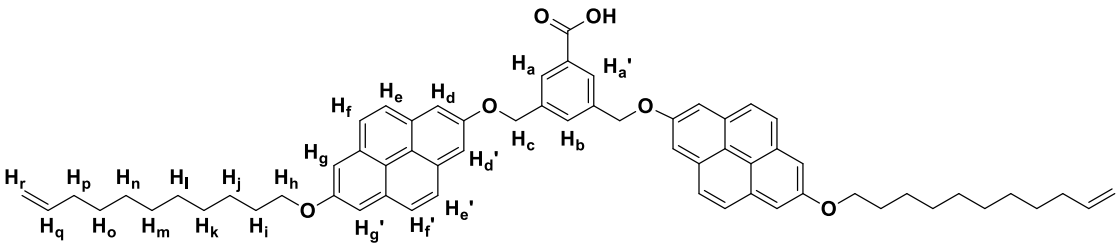

^{1}H NMR (400 MHz, $CDCl_3$) δ 8.26 (s, 2H, Ha+a'), 8.01 (s, 1H, Hb), 7.95 – 7.86 (m, 8H, He+e'+ f+f'), 7.73 (s, 4H, Hd+d'), 7.67 (s, 4H, Hg+g'), 5.82 (ddt, *J* = 16.9, 10.1, 6.6 Hz, 2H, Hq), 5.42 (s, 4H, Hc), 5.04 – 4.84 (m, 4H, Hr), 4.24 (t, *J* = 6.7 Hz, 4H, Hh), 2.05 (q, *J* = 6.5 Hz, 4H, Hp), 1.92 (p, *J* = 6.7 Hz, 4H, Hi), 1.56 (p, *J* = 7.3 Hz, 4H, Hj), 1.48 – 1.27 (m, 20H, Hk+l+m+n+o). ^{13}C NMR (101 MHz, $CDCl_3$) δ 168.5, 156.8, 156.0, 139.3, 138.2, 131.8, 131.7, 131.6, 131.5, 128.5, 127.6, 127.4, 127.4, 127.3, 120.4, 120.0, 114.2, 112.0, 111.6, 111.4, 111.3, 69.9, 68.7, 33.9, 29.6, 29.5, 29.2, 29.0, 26.2. MALDI calcd. for C63H66O6 (M): 918.5; Found: 904.5.

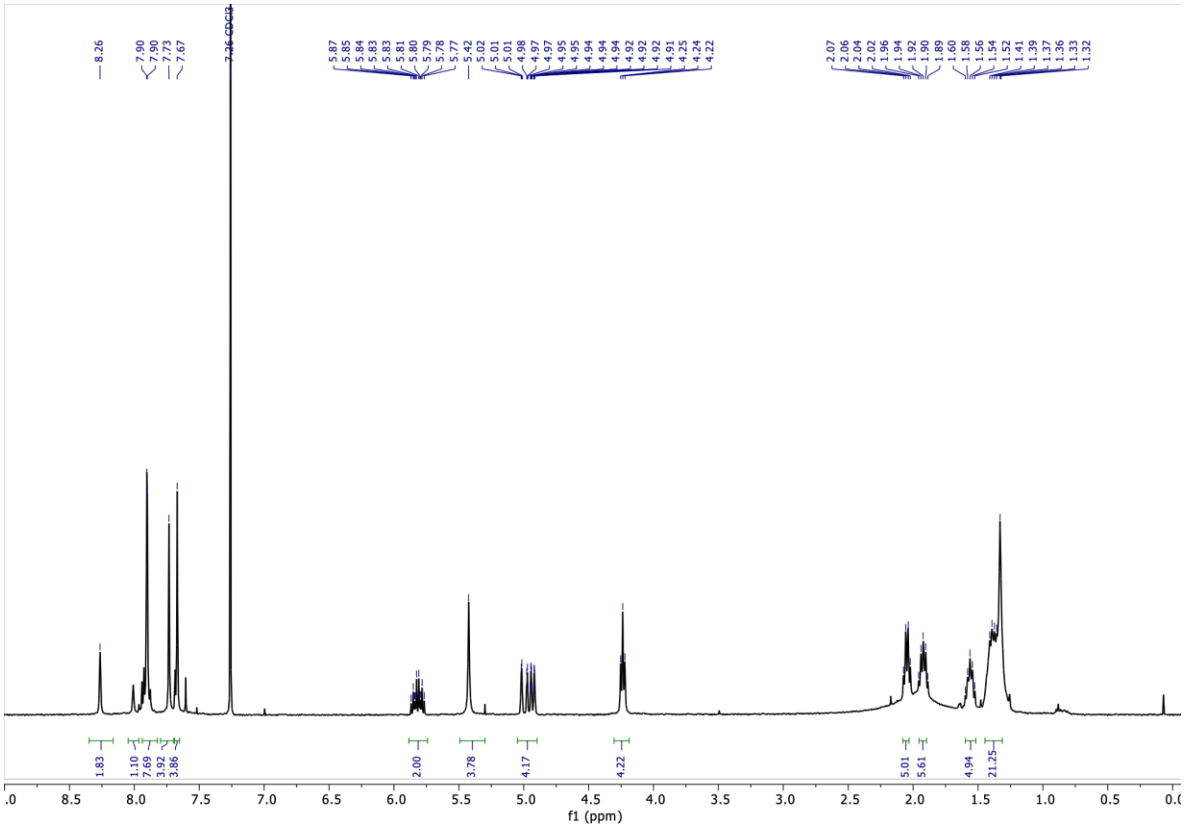

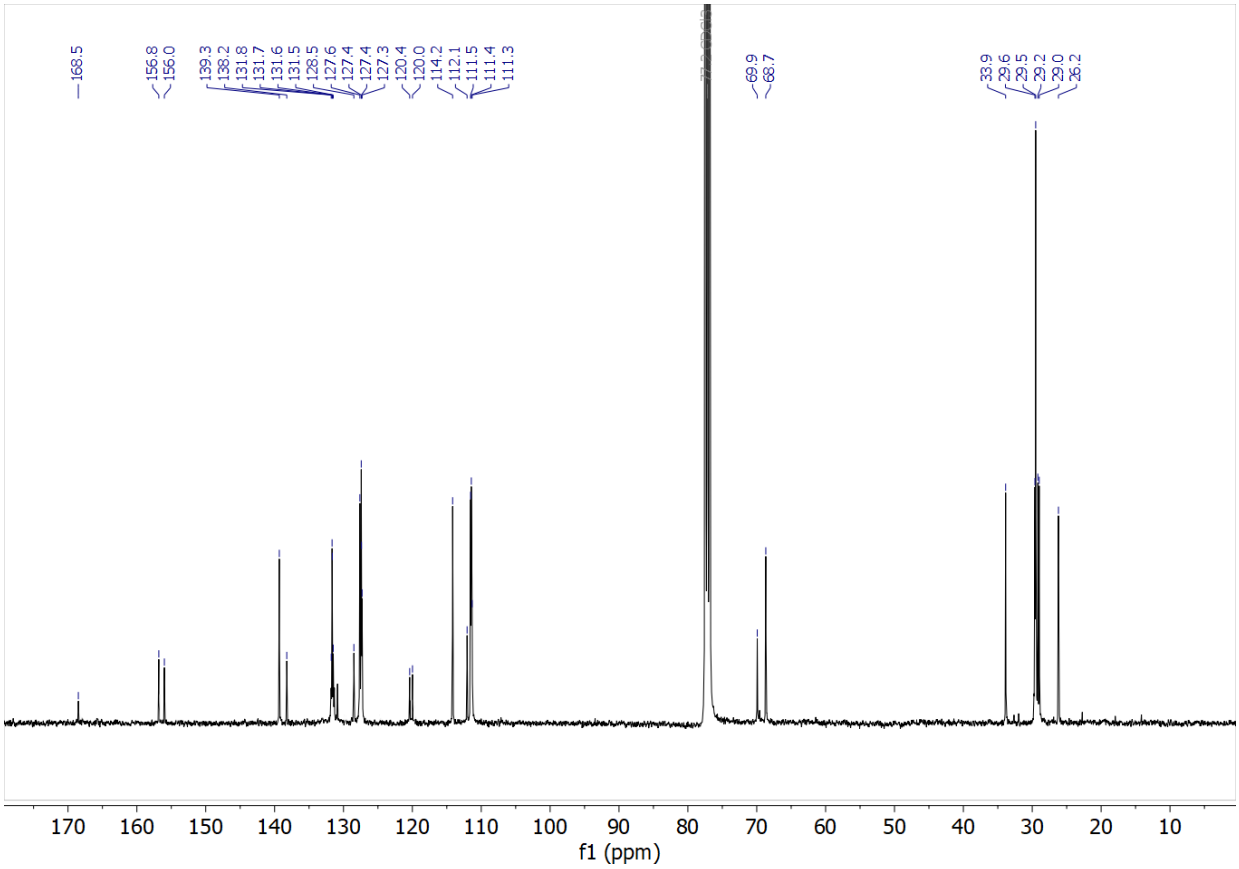
168.5
156.8
156.0
139.3
138.2
131.8
131.7
131.6
131.5
128.5
127.6
127.4
127.4
127.3
120.4
120.0
114.2
112.1
111.5
111.4
111.3
69.9
68.7
33.9
29.6
29.5
29.2
29.0
26.2
170 160 150 140 130 120 110 100 90 80 70 60 50 40 30 20 10
f1 (ppm)

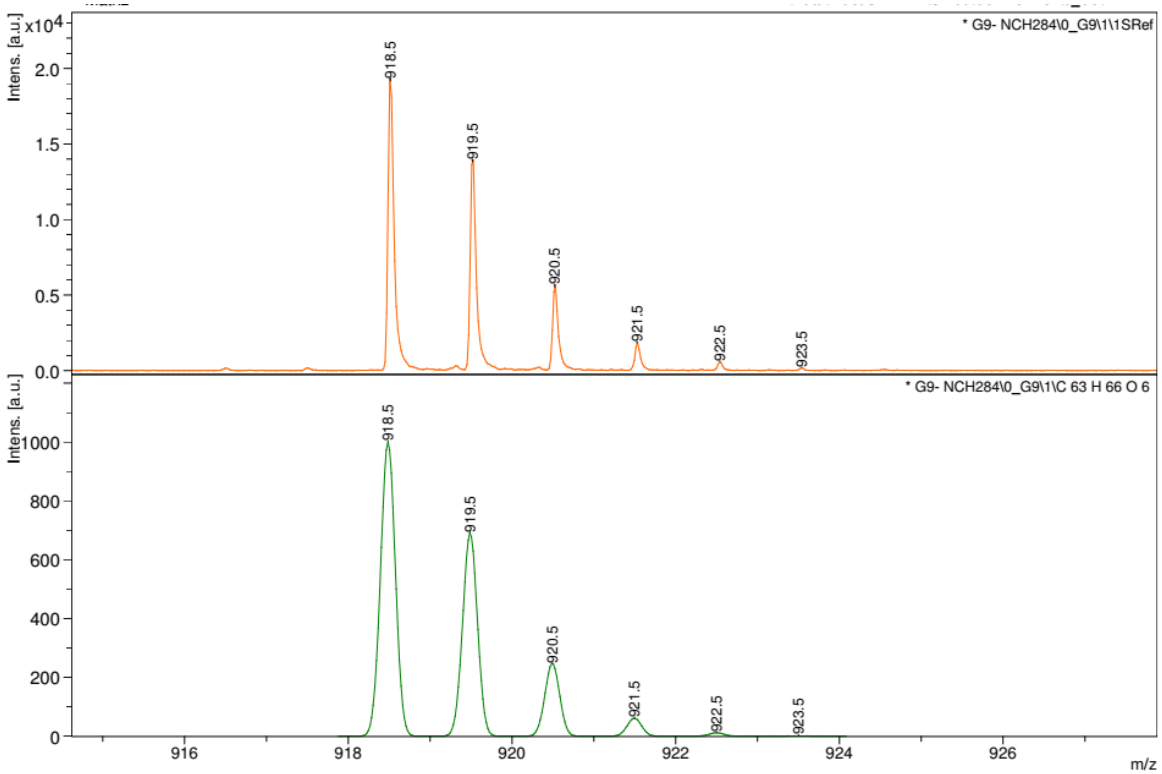
Intens. [a.u.]
x10^4
2.0
1.5
1.0
0.5
0.0
* G9- NCH284\0_G9\1\1SRef
918.5
919.5
920.5
921.5
922.5
923.5
Intens. [a.u.]
1000
800
600
400
200
0
* G9- NCH284\0_G9\1\C 63 H 66 O 6
918.5
919.5
920.5
921.5
922.5
923.5
916
918
920
922
924
926
m/z

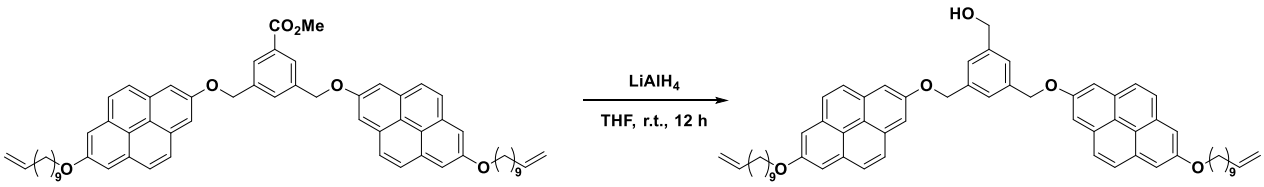

(3,5-bis(((7-(undec-10-en-1-yloxy)pyren-2-yl)oxy)methyl)phenyl)methanol. methyl 3,5-bis(((7-(undec-10-en-1-yloxy)pyren-2-yl)oxy)methyl)benzoate (270 mg, 0.29 mmol, 1 eq) was dissolved in 5 mL of THF at 0°C. Over this solution 570 µL (0.57 mmol, 2 eq) of 1M $LiAlH_4$ in THF were added and the reaction was stirred for 12 h at room temperature. After this time water was carefully added and the solid was recovered by filtration. The solid was washed with water and cold methanol to afford the pure product (245 mg, 92% yield).

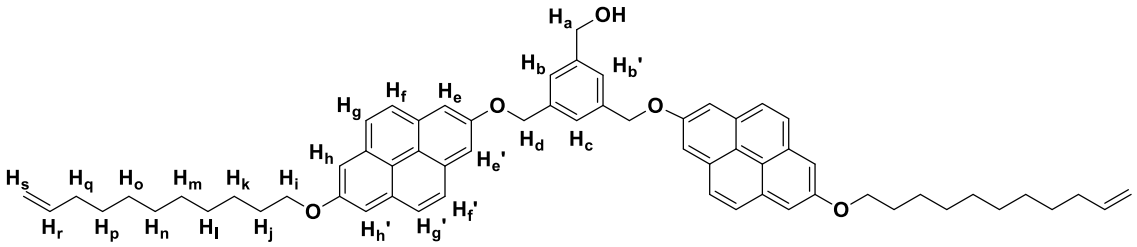

^{1}H NMR (400 MHz, $CDCl_3$) δ 7.91 (s, 8H, Hf+f'+g+g'), 7.75 (s, 4H, He+e'), 7.68 (s, 6H, Hh+h'+b+b'), 7.56 (s, 1H, Hc), 5.82 (ddt, *J* = 17.0, 10.3, 6.7 Hz, 2H, Hr), 5.39 (s, 4H, Hd), 5.10 – 4.88 (m, 4H, Hs), 4.80 (s, 2H, Ha), 4.24 (t, *J* = 6.5 Hz, 4H, Hi), 2.05 (q, *J* = 6.4 Hz, 4H, Hq), 1.92 (q, *J* = 6.8 Hz, 4H, Hj), 1.64 – 1.49 (m, 8H, Hk+p), 1.33 (m, 16H, Hl+m+n+o). ^{13}C NMR (101 MHz, $CDCl_3$) δ 157.0, 156.3, 139.4, 138.3, 131.8, 127.7, 127.6, 125.7, 120.5, 120.1, 114.3, 111.7, 111.6, 70.5, 68.8, 65.3, 34.0, 29.7, 29.6, 29.3, 29.1, 26.3. MALDI calcd. for C63H68O5 (M): 904.5; Found: 904.5.

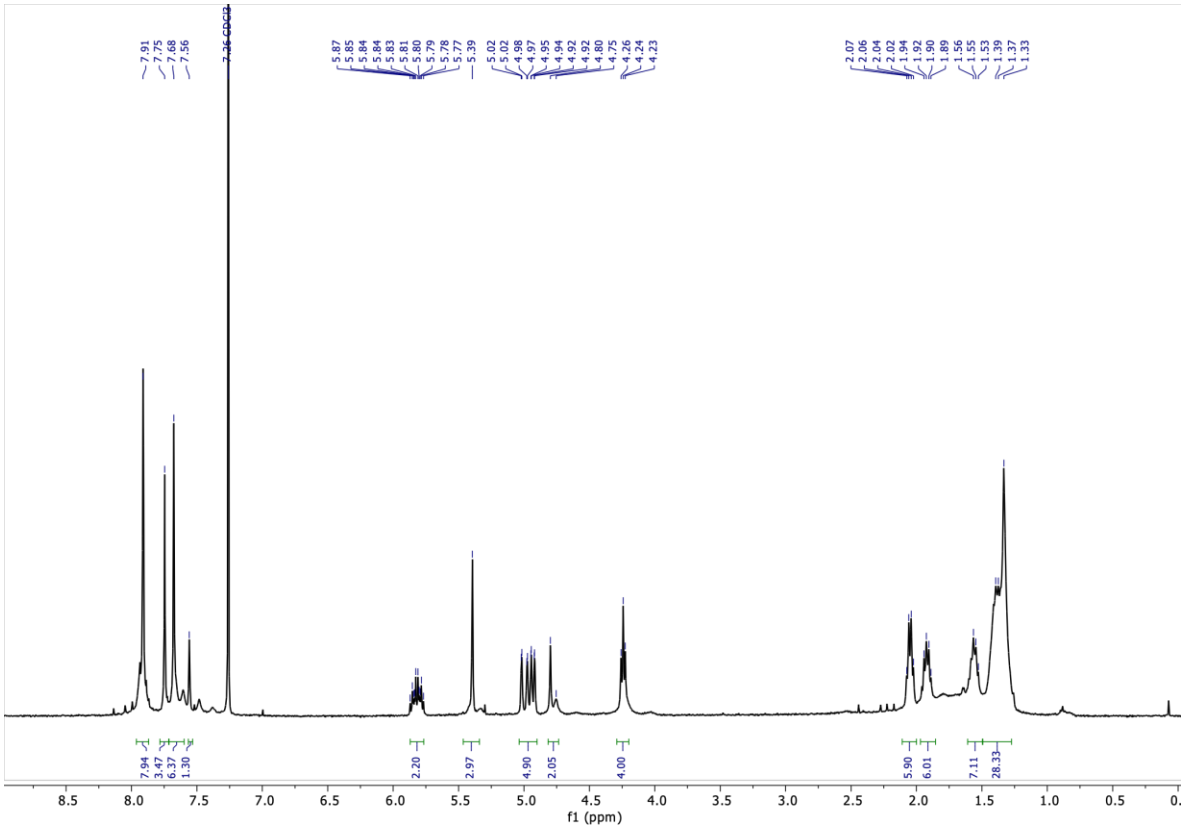

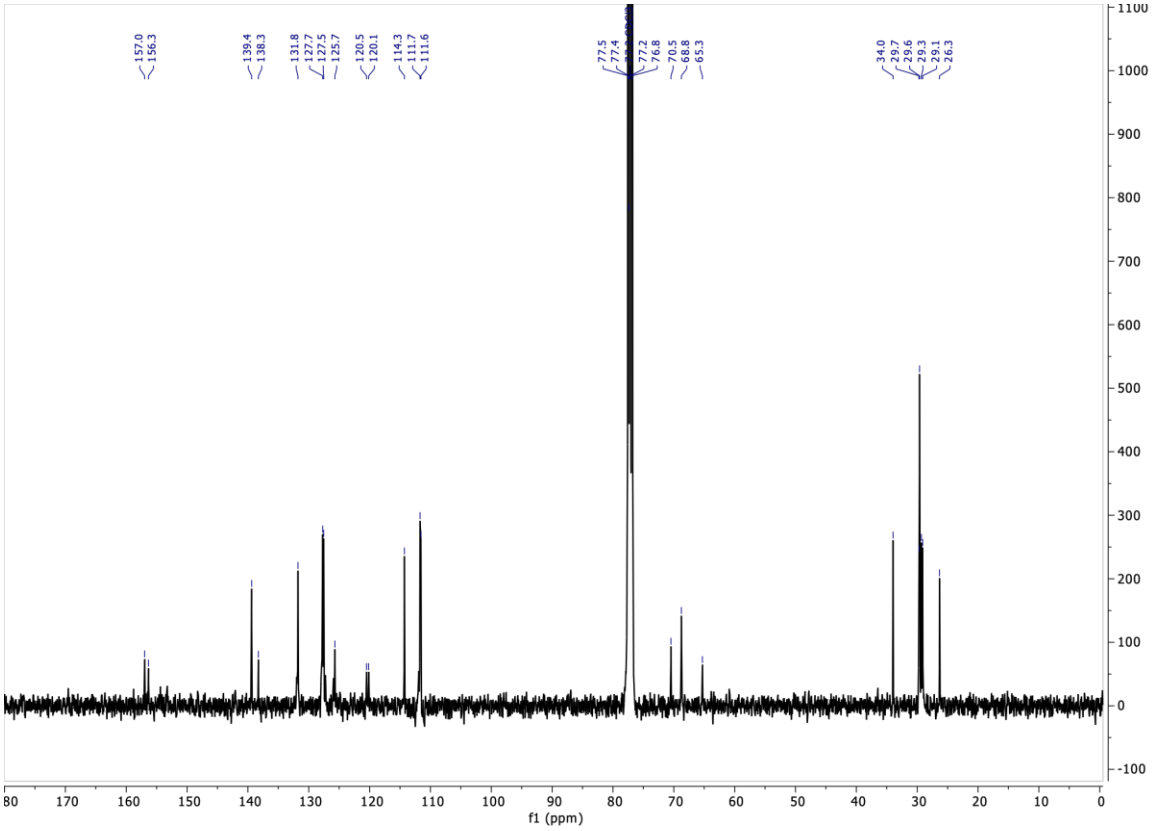
157.0
156.3
139.4
138.3
131.8
127.7
127.5
125.7
120.5
120.1
114.3
111.7
111.6
77.5
77.4
77.2
76.8
70.5
68.8
65.3
34.0
29.7
29.6
29.3
29.1
26.3
f1 (ppm)

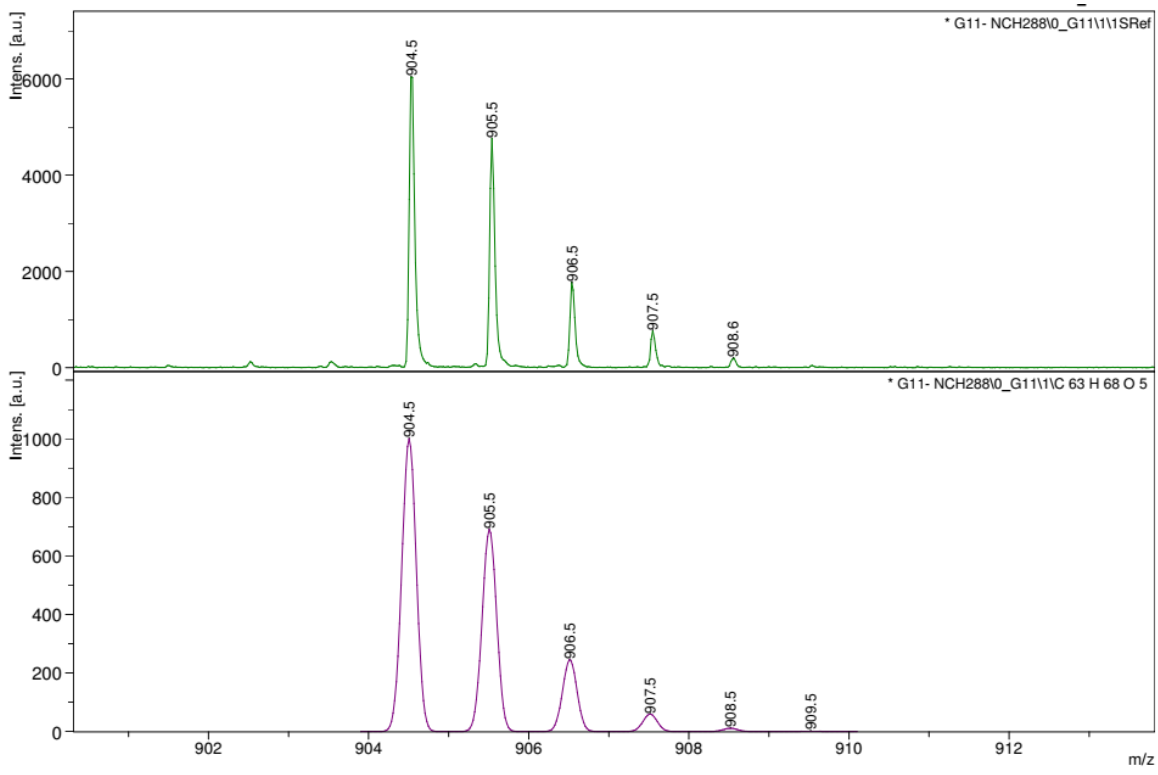
* G11- NCH288\0_G11\1\1SRef
Intens. [a.u.]
904.5
905.5
906.5
907.5
908.6
* G11- NCH288\0_G11\1\C 63 H 68 O 5
Intens. [a.u.]
904.5
905.5
906.5
907.5
908.5
909.5
m/z

3. Preparation and characterization of MINTs

MINT forming reaction **[S2]** was carried out using a commercially available ball mill (Fritsch PULVERISETTE 7) equipped with stainless steel reactors and balls. 50 mg of SWCNTs, 0.48 µmol/mg U-shape and 0.1 µmol/ U-Shape µmol of Grubbs catalyst 2nd gen. were placed in 20 mL stainless steel reactors containing 2 stainless steel balls (10 mm in diameter) and 0.4 mL of toluene. The mixture was milled for 5 min at 150 rpm. After each milling experiment, the resulting powder was collected, and the unreacted U-shapes and Grubbs' catalyst were removed by three washes in DCM, in which we suspended the product in 20 mL of DCM with 5 minutes of bath sonication and then filtered the solid through a 0.2 µm pore PTFE membrane. All the samples were full characterised using TGA, UV-vis-NIR and Raman spectroscopies.

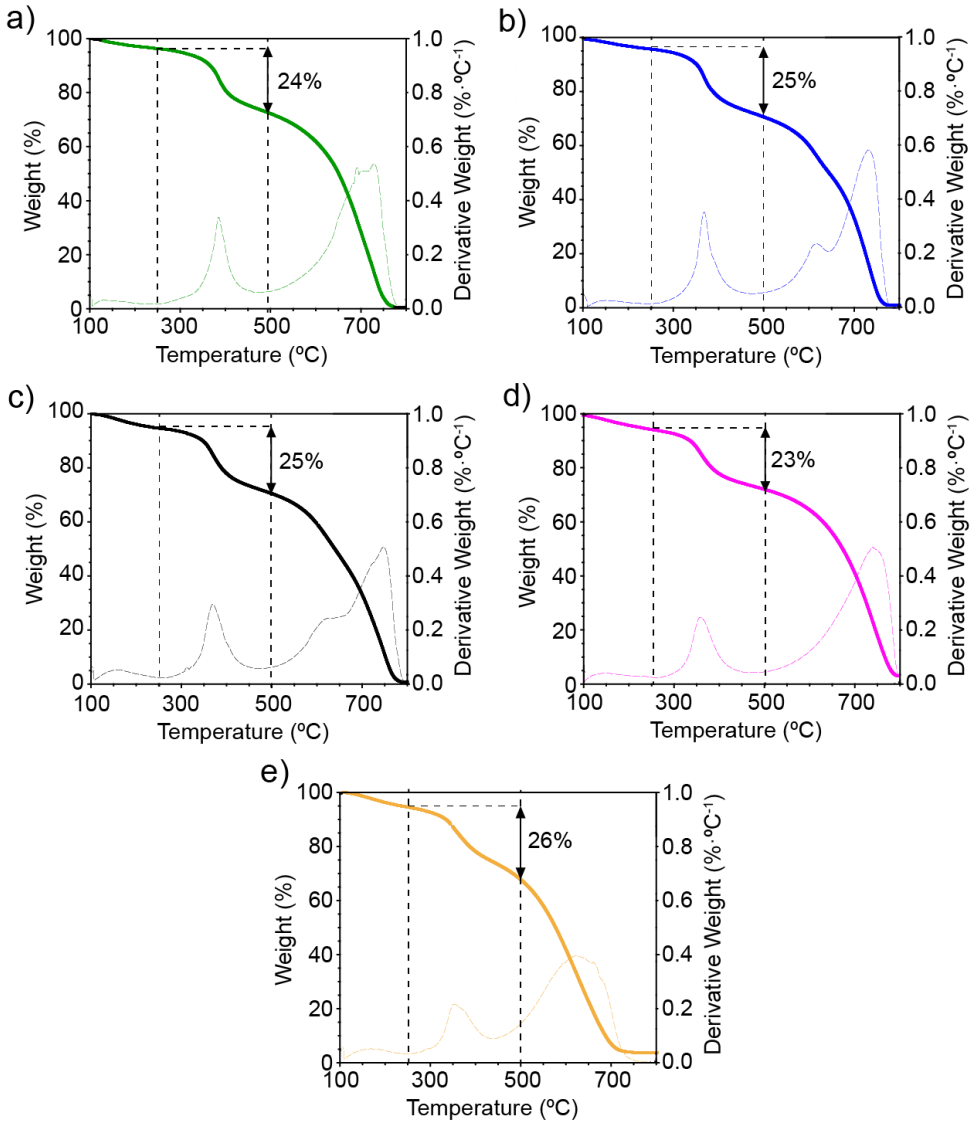

Figure S1. TGA (Air, 10 ºC·min-1) of a) $MINT_{XYLENE}$; b) $MINT_{ALKENE}$; c) $MINT_{COOMe}$; d) $MINT_{COOH}$; and e) $MINT_{OH}$.

In TGA (Air, 10 ºC·min-1) (Figure S1) we can observe a similar functionalization (23-26%) for all samples with the weight loss associated to the organic material centered at 370-380 ºC.

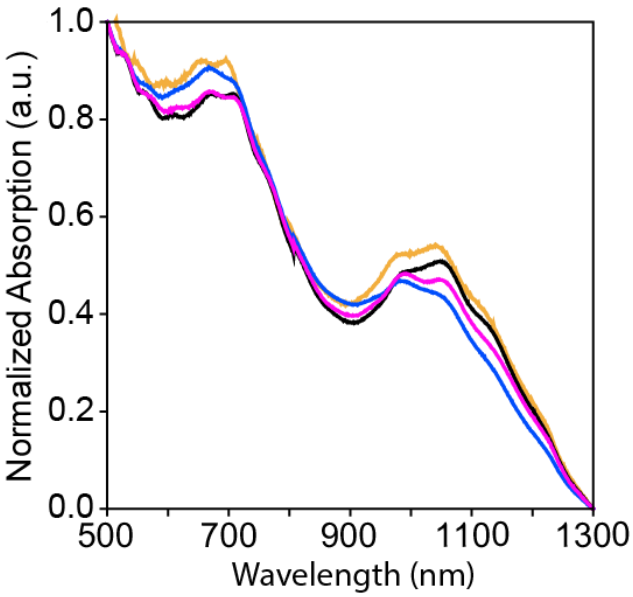

Figure S2. UV/Vis/NIR spectra (D2O, 1 % sodium dodecyl sulfate (SDS), 298 K) of $MINT_{ALKENE}$ (blue); $MINT_{COOMe}$ (black); $MINT_{COOH}$ (pink); and $MINT_{OH}$ (yellow)

UV-vis-NIR extinction spectra of MINTs all taken in D2O with 1 % sodium dodecyl sulfate (SDS) at room temperature, are shown in Figure S2. The spectra show a very efficient individualization of the SWNTs and well-defined interband absorption peaks are observed. No significant differences can be observed for the different MINTs samples.

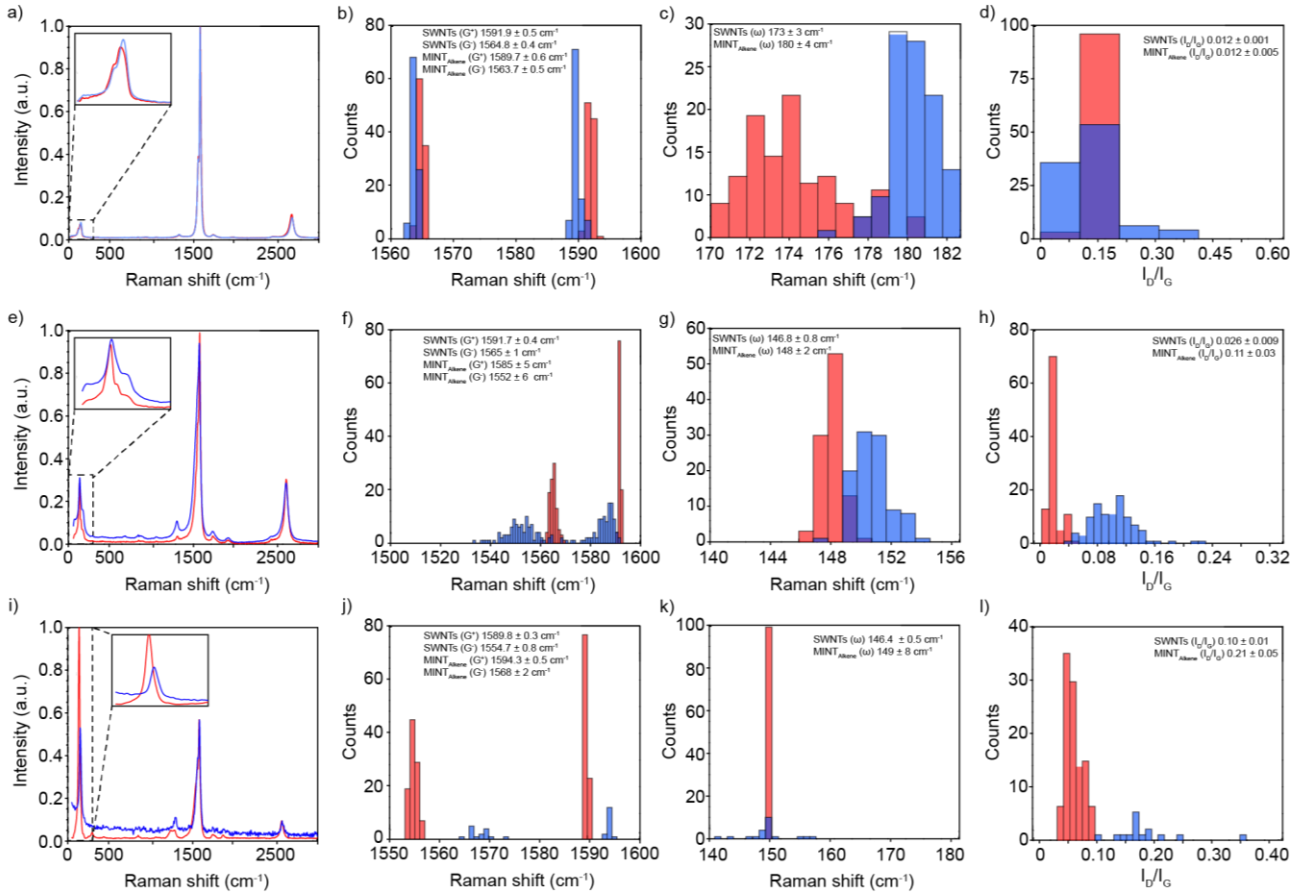

Figure S3. Raman spectra of SWCNTs (red) and $MINT_{ALKENE}$ (blue). a) Average Raman spectra (λ=532 nm); b) G band shift (λ=532 nm); c) RBM shift (λ=532 nm); d) Intensity ratio Id/Ig (λ=532 nm); e) Average Raman spectra (λ=633 nm); f) G band shift (λ=633 nm); g) RBM shift (λ=633 nm); h) Intensity ratio Id/Ig (λ=633 nm); i) Average Raman spectra (λ=785 nm); j) G band shift (λ=785 nm); k) RBM shift (λ=785 nm); and l) Intensity ratio Id/Ig (λ=785 nm).

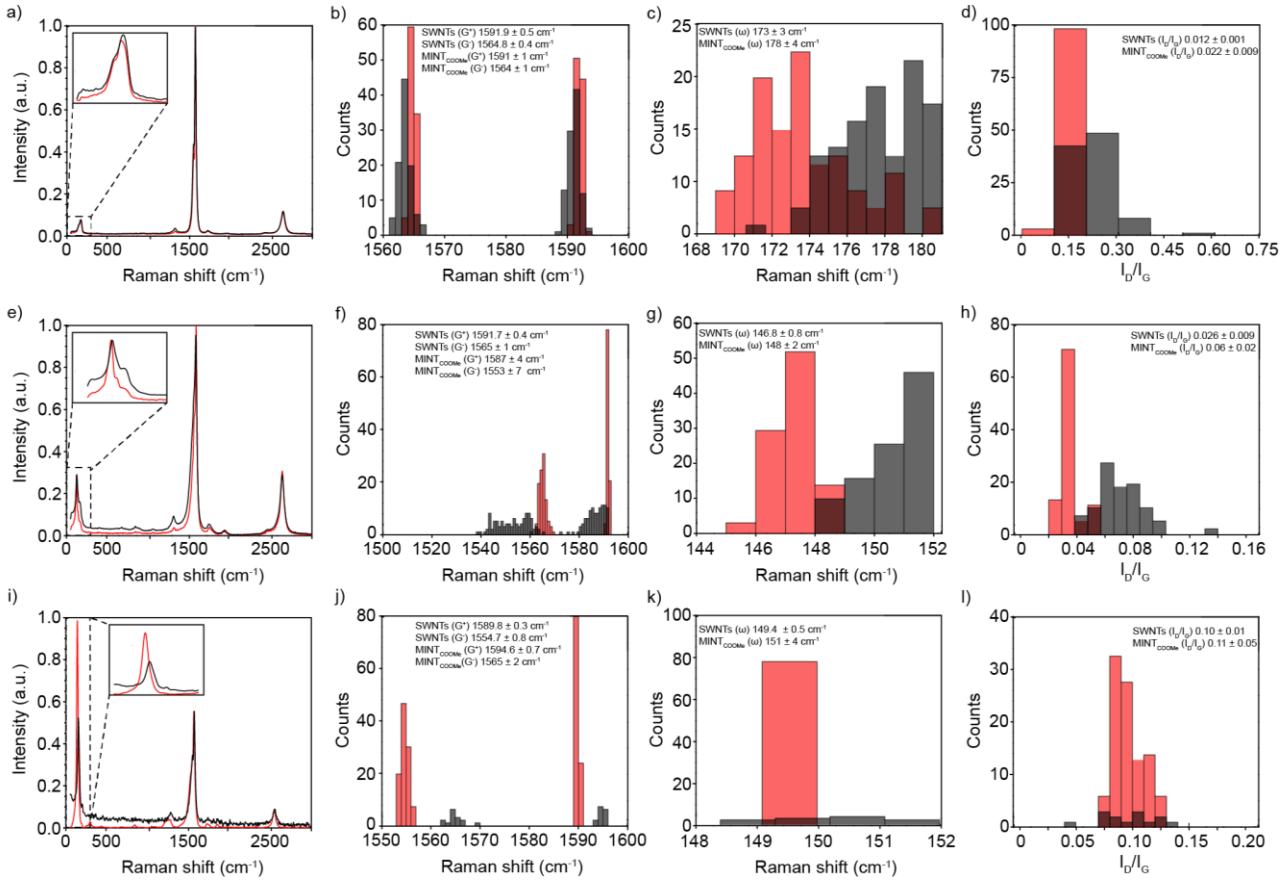

Figure S4. Raman spectra of SWCNTs (red) and $MINT_{COOMe}$ (black). a) Average Raman spectra (λ=532 nm); b) G band shift (λ=532 nm); c) RBM shift (λ=532 nm); d) Intensity ratio Id/Ig (λ=532 nm); e) Average Raman spectra (λ=633 nm); f) G band shift (λ=633 nm); g) RBM shift (λ=633 nm); h) Intensity ratio Id/Ig (λ=633 nm); i) Average Raman spectra (λ=785 nm); j) G band shift (λ=785 nm); k) RBM shift (λ=785 nm); and l) Intensity ratio Id/Ig (λ=785 nm).

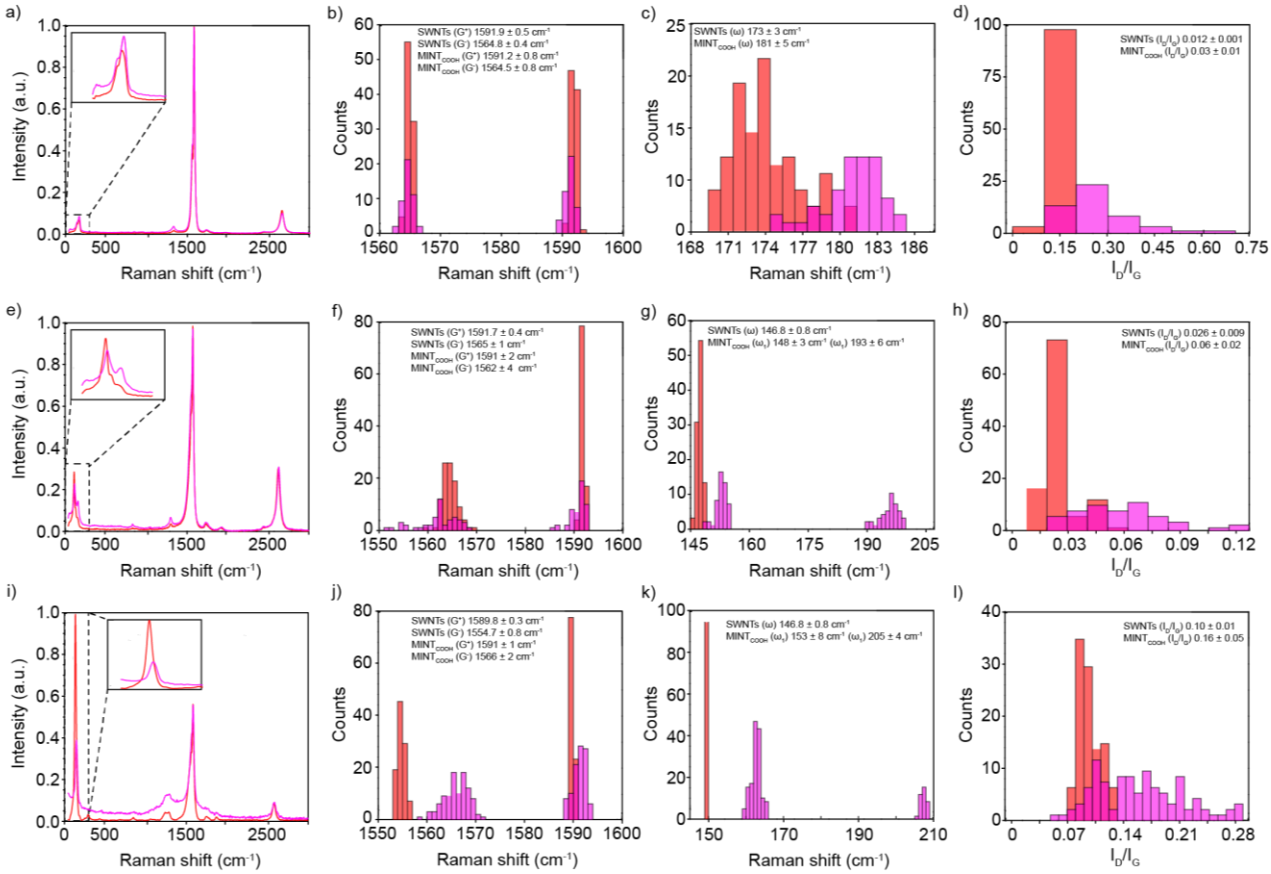

Figure S5. Raman spectra of SWCNTs (red) and MINT$_{COOH}$ (pink). a) Average Raman spectra (λ=532 nm); b) G band shift (λ=532 nm); c) RBM shift (λ=532 nm); d) Intensity ratio Id/Ig (λ=532 nm); e) Average Raman spectra (λ=633 nm); f) G band shift (λ=633 nm); g) RBM shift (λ=633 nm); h) Intensity ratio Id/Ig (λ=633 nm); i) Average Raman spectra (λ=785 nm); j) G band shift (λ=785 nm); k) RBM shift (λ=785 nm); and l) Intensity ratio Id/Ig (λ=785 nm).

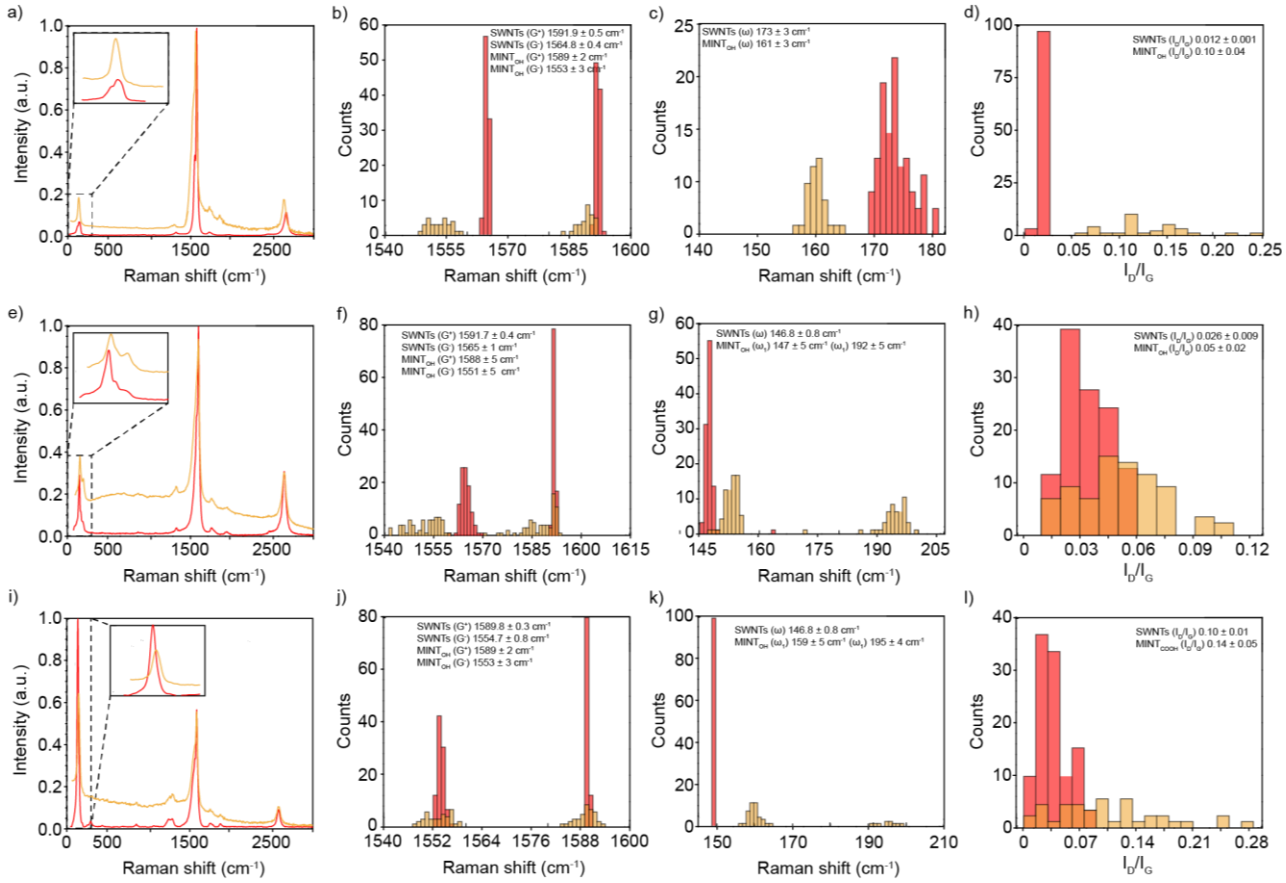

Figure S6. Raman spectra of SWCNTs (red) and $MINT_{OH}$ (yellow). a) Average Raman spectra (λ=532 nm); b) G band shift (λ=532 nm); c) RBM shift (λ=532 nm); d) Intensity ratio Id/Ig (λ=532 nm); e) Average Raman spectra (λ=633 nm); f) G band shift (λ=633 nm); g) RBM shift (λ=633 nm); h) Intensity ratio Id/Ig (λ=633 nm); i) Average Raman spectra (λ=785 nm); j) G band shift (λ=785 nm); k) RBM shift (λ=785 nm); and l) Intensity ratio Id/Ig (λ=785 nm).

Table S1. Summary of Raman spectroscopy data

	RBM	**G^+**	**G^-**	**I_D/I_G**
SWNTs				
λ_{exc} = 532	173±3 cm^{-1}	1591.9±0.5 cm^{-1}	1564.8±0.4 cm^{-1}	0.012±0.001 cm^{-1}
λ_{exc} = 633	146.8±0.8 cm^{-1}	1591.7±0.4 cm^{-1}	1565±1 cm^{-1}	0.026±0.009 cm^{-1}
λ_{exc} = 785	146.4±0.5 cm^{-1}	1589.8±0.3 cm^{-1}	1554.7±0.8 cm^{-1}	0.10±0.01 cm^{-1}
$MINT_{ALKENE}$				
λ_{exc} = 532	180±4 cm^{-1}	1589.7±0.6 cm^{-1}	1563.7±0.5 cm^{-1}	0.012±0.005 cm^{-1}
λ_{exc} = 633	148±2 cm^{-1}	1585±5 cm^{-1}	1552±6 cm^{-1}	0.11±0.03 cm^{-1}
λ_{exc} = 785	149±8 cm^{-1}	1594.3.8±0.5 cm^{-1}	1568±2 cm^{-1}	0.21±0.05 cm^{-1}

MINT$_{COOMe}$				
λ_{exc} = 532	178±4 cm^{-1}	1591±1 cm^{-1}	1564±1 cm^{-1}	0.022±0.009 cm^{-1}
λ_{exc} = 633	148±2 cm^{-1}	1587±4 cm^{-1}	1553±7 cm^{-1}	0.06±0.02 cm^{-1}
λ_{exc} = 785	151±4 cm^{-1}	1594.6±0.7 cm^{-1}	1565±2 cm^{-1}	0.11±0.05 cm^{-1}
MINT$_{COOH}$				
λ_{exc} = 532	181±5 cm^{-1}	1591.2±0.8 cm^{-1}	1564.5±0.8 cm^{-1}	0.03±0.01 cm^{-1}
λ_{exc} = 633	(1) 148±3 cm^{-1} (2) 193±6 cm^{-1}	1591±2 cm^{-1}	1562±4 cm^{-1}	0.06±0.02 cm^{-1}
λ_{exc} = 785	(1) 153±8 cm^{-1} (2) 205±4 cm^{-1}	1591±1 cm^{-1}	1566±2 cm^{-1}	0.16±0.05 cm^{-1}
MINT$_{OH}$				
λ_{exc} = 532	161±3 cm^{-1}	1589±2 cm^{-1}	1553±3 cm^{-1}	0.10±0.04 cm^{-1}
λ_{exc} = 633	(1) 147±5 cm^{-1} (2) 192±5 cm^{-1}	1588±5 cm^{-1}	1551±5 cm^{-1}	0.05±0.02 cm^{-1}
λ_{exc} = 785	(1) 159±5 cm^{-1} (2) 195±4 cm^{-1}	1589±2 cm^{-1}	1553±3 cm^{-1}	0.14±0.05 cm^{-1}

Average Raman spectra of the SWCNT (black) compared to the MINTs are included in Figures S3-6 with zoom into RBM region are included in Figure S S3-6 together with histograms of intensity ratio (Id/Ig), D, G band position of the individual spectra for three different excitation wavelength (532 nm in a-d, 633 nm in e-h) and 785 nm in i-l). The histograms are obtained by extracting for each individual spectrum used in the averages, the position of the bands and the intensity ratio between D and G modes. All data is summarized in Table S1.

The radial breathing modes (RBM) are related with the contraction and expansion of the tubes, and hence, associated to the diameter and aggregation state. All samples follow a general trend. No significant shift of the D and G modes is found between the pristine tubes and the MINTs. The intensity ratio between D and G bands (I_d/I_g) is slightly higher in the MINTs samples, as expected for the mechanochemical preparation of MINTs but not significantly important in this work. Regarding the RBM, all samples present a blue shift upon functionalization, which matches with the functionalization of smaller carbon nanotubes diameters. Similar shifts to higher frequencies are also observed in the RBMs the three laser and are indicative of a hardening of the radial vibrations of the SWCNTs which is a reasonable consequence of surrounding their structure with macrocycles.

4. Preparation and characterization of sensing layers: profilometry and exposure to gas

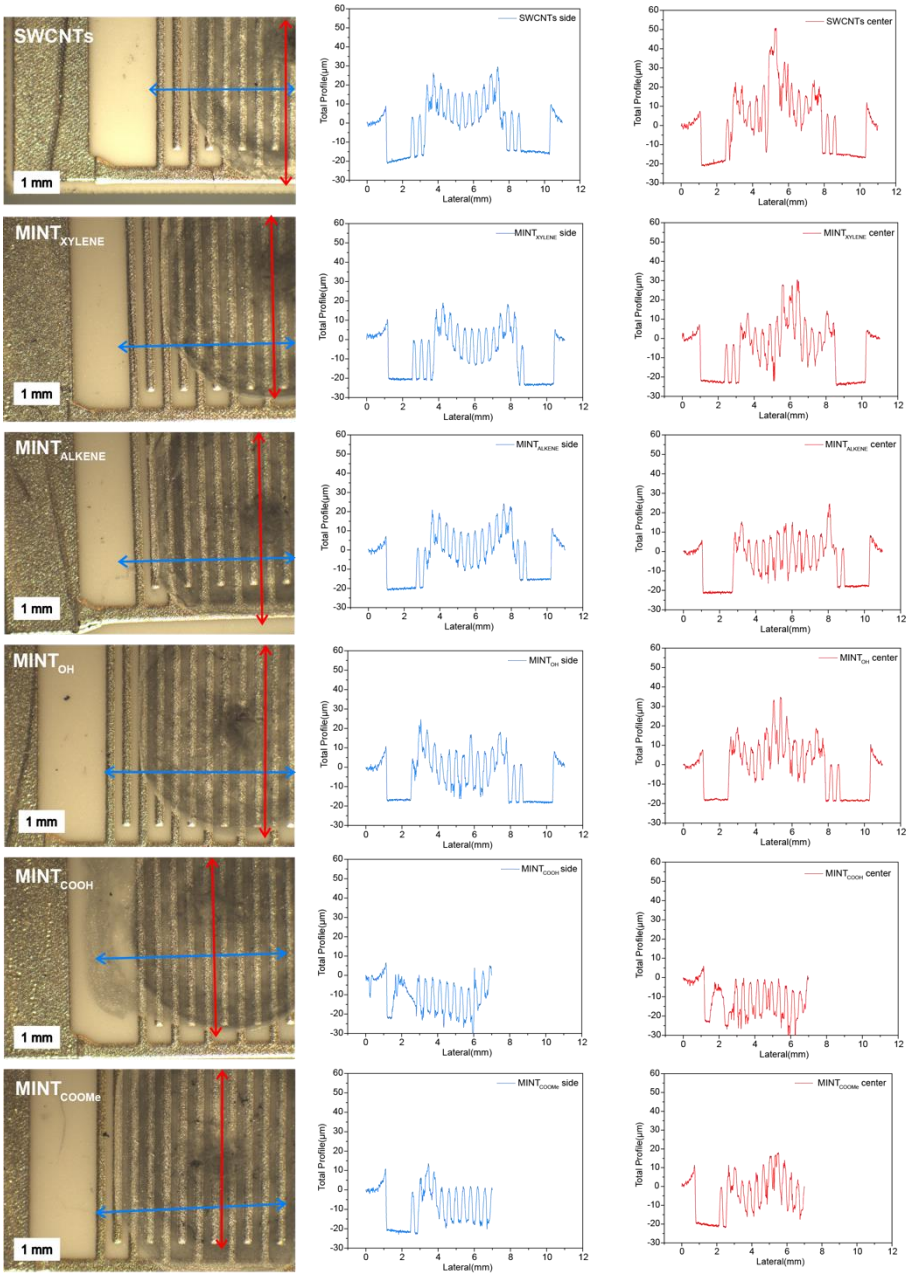

Fig.S7 Profilometry analysis of sensing layers.

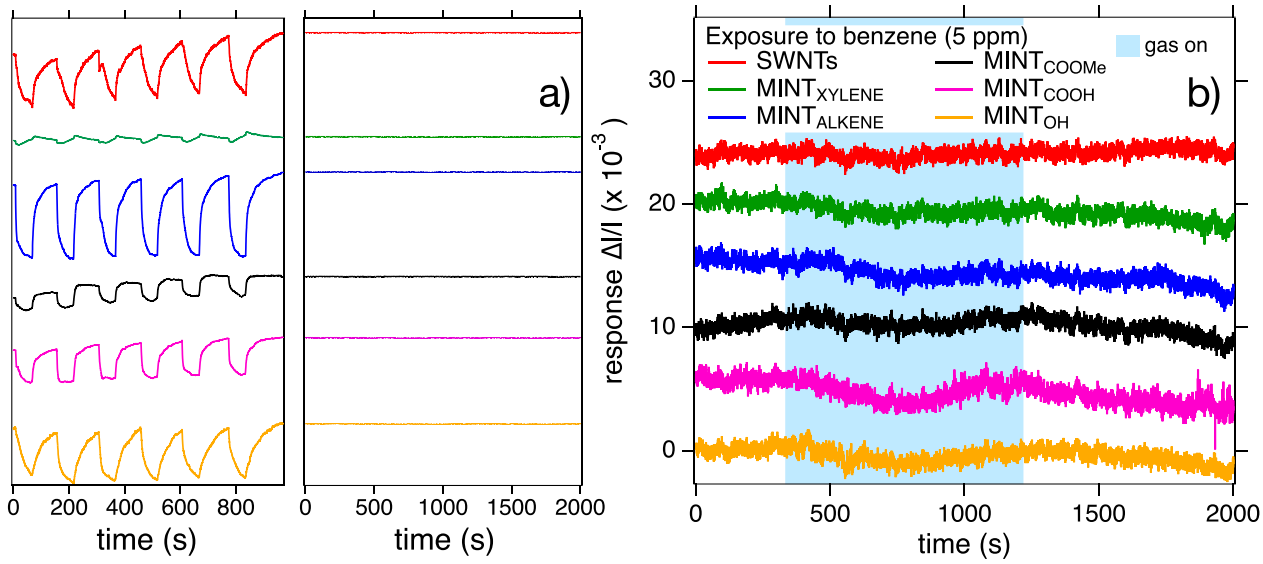

Fig. S8. Dynamical response of sensing layers upon exposure to C_6H_6. Left panel: exposure to NH_3, mid-panel exposure to benzene (on the same vertical scale of left panel), right panel: enlarged view of mid panel.

Table S2. LOD for ammonia exposures

Ammonia	Sigma (μA)	LOD (ppb)	ΔLOD/LOD %
SWNTs	43	30	126%
$MINT_{XYLENE}$	110	42	81%
$MINT_{ALKENE}$	132	2	118%
$MINT_{COOMe}$	138	22	50%
$MINT_{COOH}$	81	10	74%
$MINT_{OH}$	93	30	144%

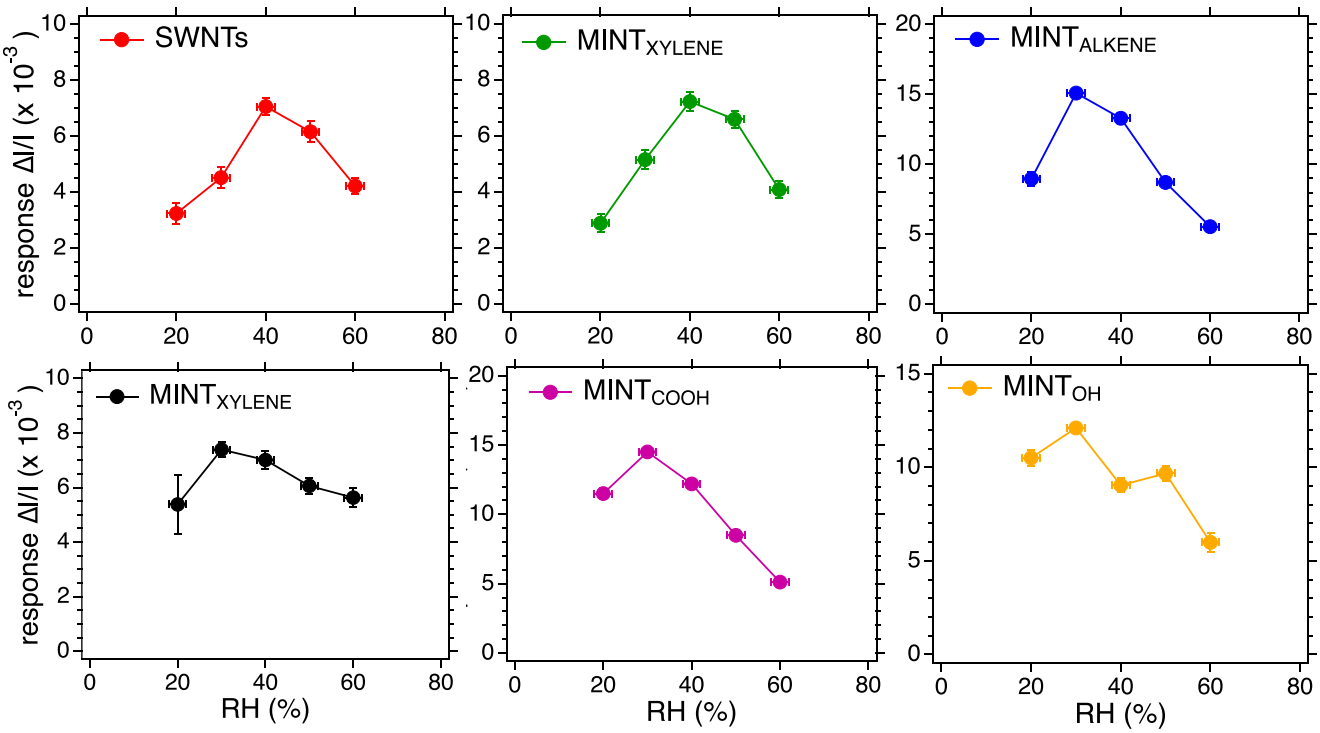

Fig. S9. Response to 2 ppm ammonia under different R.H. conditions.

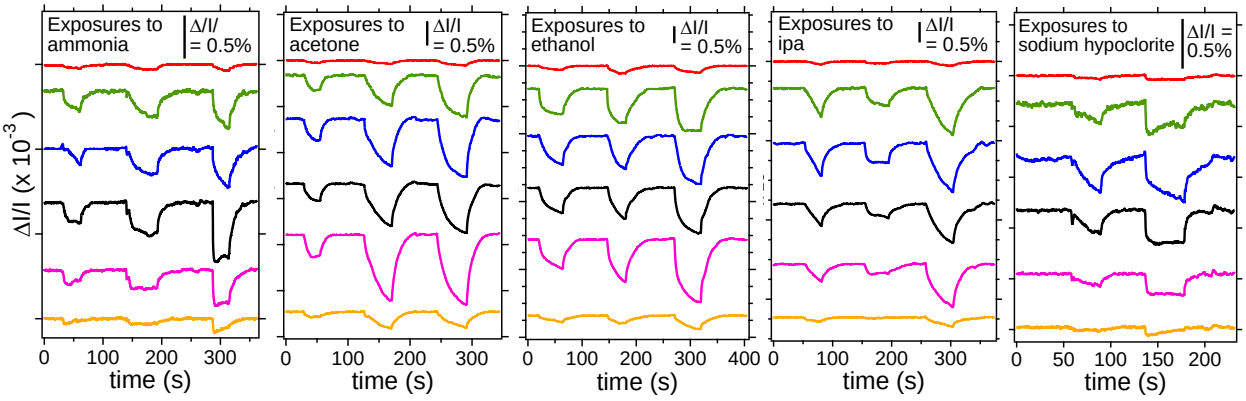

Fig. S10. Dynamic response of sensing layers after 270 days.

For each target gas, three exposures were taken at increasing concentration values, c_0, $4c_0$, and $6c_0$, where c_0 was set at 16 ppm for NH_3, 100 ppm for acetone, 100 ppm for EtOH, 100 ppm for IPA, 100 ppm for NaClO (only c_0 and4 c_0 for this analyte). Dynamical response curves for NO_2 are shown in Fig. S11.

Table S3. Sensors baseline resistance R_0 variation over time (0-270 days).

	Initial Resistance (Ω)	Resistance after 270 days (Ω)	Variation (Ω)	Relative Variation (%)
SWNTs	652	412	240	36.8%
$MINT_{XYLENE}$	2829	2305	523	18.5%
$MINT_{ALKENE}$	1416	1025	391	27.6%
$MINT_{COOMe}$	2317	1704	614	26.5%
$MINT_{COOH}$	1677	1235	442	26.4%
$MINT_{OH}$	1159	772	387	33.4%

The largest change of baseline resistance R_0 after 270 days is detected for SWNTs and $MINT_{OH}$, i.e. 36,8 % and 33,4%, respectively. Incidentally, we also note that these sensing layers are those with the lowest sensitivities to NH_3, acetone, EtOH, IPA, and NaClO among the present set of sensing layers. For all the other samples, the relative change of baseline resistance ranged from 18.5% to 27.6 %. Based on the results of the resistivity network model presented below (Fig.S12), such changes of baseline resistance are expected to yield a decrease of sensitivity well below 10%.

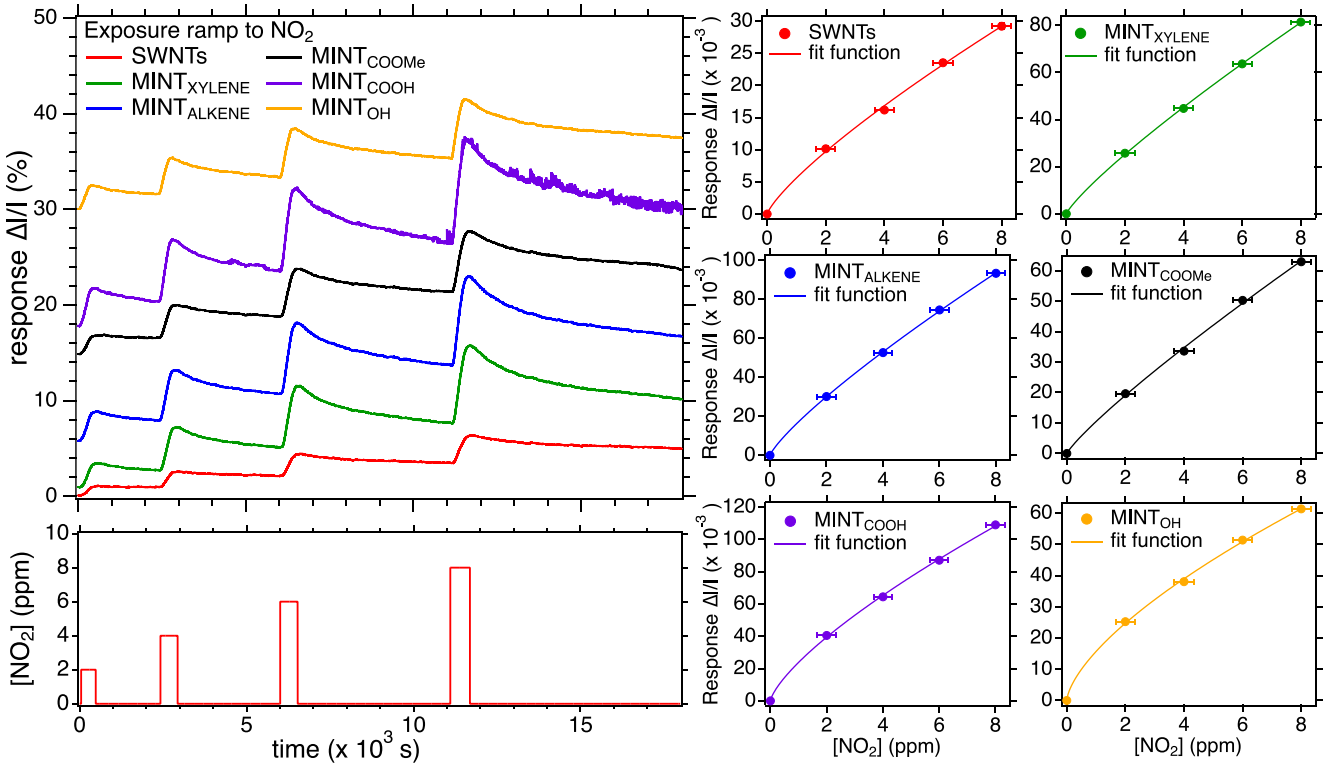

Fig.S11 Dynamical responses and calibration curves for NO_2 exposure in the 2-8 ppm range.

Table S4. Results of the Freundlich fit of the calibration curves obtained for NO_2.

	A ($x10^{-3}$)	ΔA ($x10^{-4}$)	n	Δn
SWNTs	5.6	3	0.79	0.03
$MINT_{XYLENE}$	14.1	2	0.84	0.01
$MINT_{ALKENE}$	17.0	1	0.82	0.01
$MINT_{COOMe}$	10.5	5	0.86	0.03
$MINT_{COOH}$	23.8	7	0.73	0.02
$MINT_{OH}$	15.7	5	0.65	0.02

5. SWNTs layer as a net of resistors in parallel

In order explore the effects of baseline resistivity (R_0) changes on the response of a CNTs, we assumed that the sensing layer can be modelled with a network of resistors connected in parallel. Therefore, upon gas molecule adsorption on one of the CNTs in the network, a change of resistivity of this single resistor is expected. This, in turn, will affect the overall resistance of the layer. Within the network of parallel resistances we set:

$$R_0 = R_{eq} = \left(\sum_{k=1}^{N} \frac{1}{R_k} \right)^{-1}$$

We then set R_i as the resistance of a single CNT interacting with the target gas molecule. Therefore, we can estimate the change of R_0 when R_i changes to $R_i+\Delta R_i$. We can rewrite the equivalent resistance as:

$$\frac{1}{R_{eq}} = \sum_{k \neq i} \frac{1}{R_k} + \frac{1}{R_i} = \frac{1}{R_{eff}} + \frac{1}{R_i}$$

Then

$$R_{eq}(R_i) = \frac{R_{eff} R_i}{R_{eff} + R_i}$$

Under normal conditions, since all nanotubes resistances are comparable and N is very large, R_i influence on R_{eq} is almost negligible. Thus, $R_{eff} \approx R_{eq}$.

Now we can estimate the effect of R_{eff} on the sensor response $S = \frac{\Delta R_{eq}}{R_{eq}}$ during a gas exposure, when R_i is assumed to change. For notation simplicity, we set R_{eff} =R and R_i=x. Then:

$$R_{eq}(x) = \frac{Rx}{R + x}$$

When the i-th nanotube is interacting with a target gas molecule, its resistance changes to $x + \Delta x$. We then measure an overall resistance change equal to:

$$R_{eq}(x + \Delta x) = \frac{R(x + \Delta x)}{R + x + \Delta x} = \frac{Rx + R\Delta x}{R + x + \Delta x}$$

Thus, the response is:

$$S = \frac{\Delta R}{R_{eq}} = \frac{R_{eq}(x + \Delta x) - R_{eq}(x)}{R_{eq}(x)}$$

If we multiply and divide for and we assume that Δx is small, we obtain:

$$S = \frac{R_{eq}(x + \Delta x) - R_{eq}(x)}{\Delta x} \cdot \frac{\Delta x}{R_{eq}(x)} = R'_{eq}(x) \frac{\Delta x}{R_{eq}(x)}$$

where $R'_{eq}(x)$ is the first derivative of R_{eq} with respect to x. Than the response S results to be:

$$S = \frac{R}{x(R + x)} \Delta x$$

The dependence of *S* on the parameter *R* can be seen by plotting *S* vs. *R* (Figure S12).

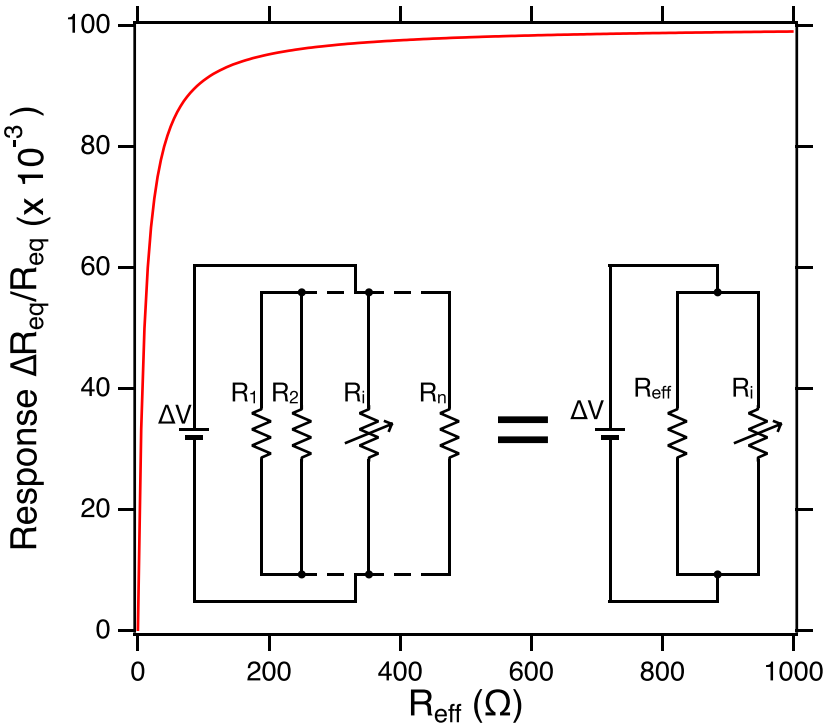

Figure S12. Response as a function of R_{eff} assuming x=10 Ω and Δx = 1 Ω as resulting from a model of the sensing layer based on a parallel resistive network upon change of the resistance of one element in the network.

The behavior of $S(R_{eff})$ indicates that the response is monotonous in R_{eff}, i.e. the greater $R_{eff} \approx R_{eq}$, the greater the response S, at a fixed value of Δx. When translated into the specific case of a SWNT network, we can conclude that the response related to the change Δx of resistance in a single tube is "amplified" when the background resistance R_{eff} is large.

6. PCA analysis for acetone-ethanol and acetone-IPA mixtures.

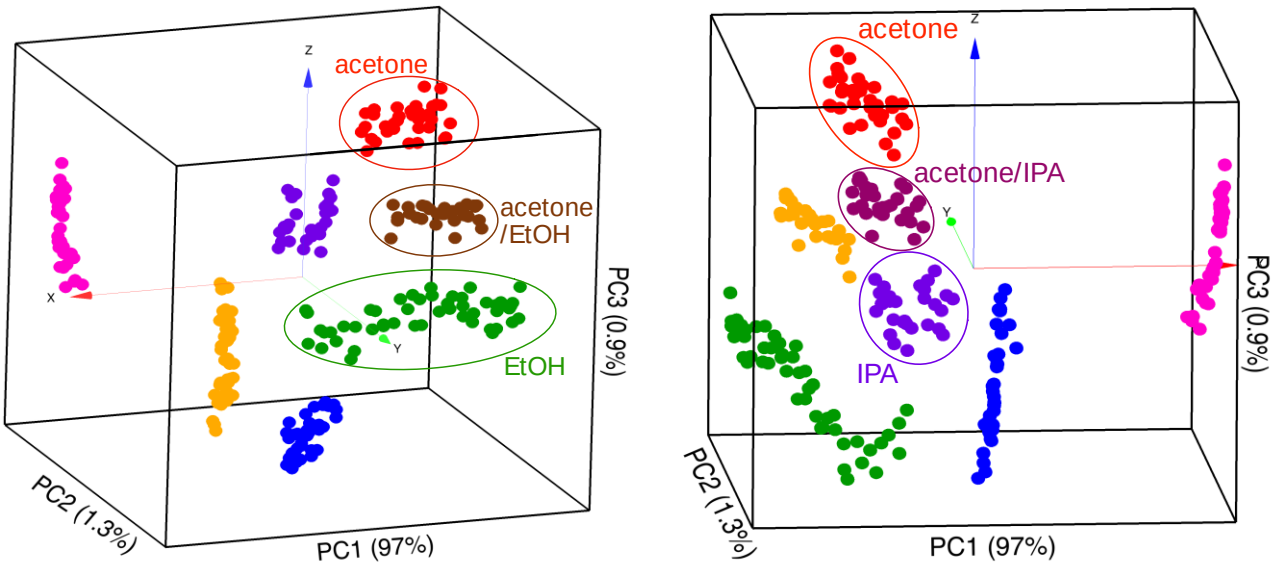

Fig.S13. PCA analysis results for the discrimination of the acetone-ethanol and acetone-IPA mixtures.

REFERENCES:

[S1] López-Moreno, A.; Pérez, E.M. Pyrene-based mechanically interlocked SWNTs. *Chem. Commun*., **2015**, 51, 5421-5424
[S2] Naranjo, A.; Jiménez, D. M.; Rivas-Caramés, M.; Villalva, J.; Ruiz-González, M.L.; Pedersen, H.; López-Moreno, A.; Pérez, E.M.; Multigram Scale Synthesis of Mechanically-Interlocked Derivatives of SWNT Using Green Mechanochemical Methods, **2024**, 10.26434/chemrxiv-2024-6q4xq
[**S3**] Zahab, A., Spina, L., Poncharal, P., & Marliere, C. Water-vapor effect on the electrical conductivity of a single-walled carbon nanotube mat. *Physical Review B*, **2000**, *62*(15), 10000.